Doctoral Dissertation
博士論文

Construction of Exact Quantum Many-Body Scar States
(厳密な量子多体傷跡状態の構成)

A Dissertation Submitted for the Degree of Doctor of Philosophy
December 2021
令和3年12月博士(理学)申請

Department of Physics, Graduate School of Science,
The University of Tokyo
東京大学大学院理学系研究科物理学専攻

Naoyuki Shibata
柴田　直幸

List of Publications

Journal Articles

[1] **Naoyuki Shibata** and Hosho Katsura, *Dissipative spin chain as a non-Hermitian Kitaev ladder*, Phys. Rev. B **99**, 174303 (2019).

[2] **Naoyuki Shibata** and Hosho Katsura, *Dissipative quantum Ising chain as a non-Hermitian Ashkin-Teller model*, Phys. Rev. B **99**, 224432 (2019).

[3] **Naoyuki Shibata**, Nobuyuki Yoshioka, and Hosho Katsura, *Onsager's Scars in Disordered Spin Chains*, Phys. Rev. Lett. **124**, 180604 (2020) [selected as **Editors' Suggestion**].

[4] Zongping Gong, Nobuyuki Yoshioka, **Naoyuki Shibata**, and Ryusuke Hamazaki, *Universal Error Bound for Constrained Quantum Dynamics*, Phys. Rev. Lett. **124**, 210606 (2020).

[5] Zongping Gong, Nobuyuki Yoshioka, **Naoyuki Shibata**, and Ryusuke Hamazaki, *Error bounds for constrained dynamics in gapped quantum systems: Rigorous results and generalizations*, Phys. Rev. A **101**, 052122 (2020).

[6] **Naoyuki Shibata** and Hosho Katsura, *Quantum Ising chain with boundary dephasing*, Progr. Theor. Exp. Phys. **2020**, 12A108.

Others

[1] [Japanese] 桶作愛喜、柴田直幸、亀井健一郎、「粒子法を用いたミルククラウン現象のシミュレーション」, スーパーコンピューティングニュース (東京大学情報基盤センタースーパーコンピューティング部門)、Vol. 18, No. 5 (2016).

[2] [Japanese] 柴田直幸、吉岡信行、桂法称、「量子の世界に「傷跡」を残す数理モデルを無限に構成する方法を発見」、東京大学大学院理学系研究科・理学部プレスリリース.

[3] [Japanese] 柴田直幸、桂法称、「オンサーガーの残した傷跡 —熱平衡化しない数理モデル—」、東京大学理学部ニュース2020年9月号.

Abstract

The eigenstate thermalization hypothesis (ETH) is known as a plausible scenario to explain thermalization of quantum systems, which states that all energy eigenstates are locally indistinguishable from the microcanonical ensemble. Although there is no rigorous proof, it is widely believed to hold for a large class of interacting systems, as evidenced by several numerical studies. Well-known exceptions are integrable and many-body localized systems. In such systems, the existence of an extensive number of conserved quantities or integrals of motions breaks ergodicity, and therefore the ETH as well. Another class of ETH-violating systems is also reported, in which the Hilbert space fractures into exponentially many disconnected subsectors.

Recently, a pioneering experiment in a Rydberg atom system revealed a mechanism of non-thermal behavior distinct from the above three. In this system, most typical states thermalize rapidly, whereas certain particular states do not for an anomalously long time. These peculiar phenomena are referred to as quantum many-body scars (QMBS), since they are reminiscent of one-body quantum scars. The experimental observation triggered a number of theoretical studies on QMBS. In particular, an effective model of this experiment, dubbed the PXP model, has been intensively studied. Another approach is to construct models with perfect QMBS, whose exact expression can be written down and perfect revivals in many-body quantum dynamics can be shown analytically. One of the examples is the exact scar states in the Affleck-Kennedy-Lieb-Tasaki (AKLT) model. Despite such intensive studies on QMBS, its general framework and origin remain unclear. Thus, we aim to expand the frontier of our understanding of these phenomena by providing a new family of analytically tractable QMBS models.

In this thesis, we propose a new class of exact QMBS models. The key to the construction is the Onsager algebra. While it was originally used to obtain exact solutions of the two-dimensional classical Ising model, we apply it to the construction of QMBS models. Our model has three remarkable features: (1) the scar states in our model are not product states but have a finite area-law entanglement. That is, our scars are not trivially ETH-violating states such as a vacuum state in the Fermi-Hubbard model. (2) Our model can be straightforwardly generalized to one with an arbitrary integer or half-integer spin quantum number. Scar states can also be generalized to multi-parameter ones. (3) We do not impose translational invariance on our model. To the best of our knowledge, this is

the first explicitly constructed example of the disordered QMBS model.

ACKNOWLEDGMENTS

I would like to express my heartfelt appreciation to my supervisor Prof. Hosho Katsura, whose insightful comments and suggestions were of inestimable value for my studies. There is no doubt that he is one of the most intelligent people I have ever discussed with. I am also deeply grateful to Dr. Nobuyuki Yoshioka. I have great respect for him not only as a talented researcher but also as a kind colleague in the same group.

I would also like to appreciate the members of the group for sharing the fulfilling days. It was great fun to hear their interesting talks in the group seminar every Wednesday.

I also thank Keiji Saito, Eiki Iyoda, Takashi Mori, Naoto Shiraishi, Ryusuke Hamazaki, and Norifumi Matsumoto for fruitful discussions.

My deepest appreciation goes to my fiancée Machiko Tamagawa, who supported me during my Ph.D. studies. This dissertation would not have been possible without her. I would also like to express my gratitude to my family for their moral support and warm encouragement.

Finally, I gratefully appreciate the financial support of the Materials Education program for the future leaders in Research, Industry, and Technology (MERIT), JSR fellowship, and JSPS.

Notations

$\mathbb{N} \coloneqq \{0, 1, 2, \dots\}$	set of natural numbers, i.e., non-negative integers
$\mathbb{R}$	set of real numbers
$\mathbb{C}$	set of complex numbers
i	imaginary unit
π	ratio of circumference of a circle to its diameter
e	Euler's number
$\delta_{jk} \coloneqq \begin{cases} 1 & j = k \\ 0 & j \neq k \end{cases}$	Kronecker delta
$\delta(\cdot)$	Dirac delta function
$[a, b] \coloneqq \{x \in \mathbb{R} \mid a \leq x \leq b\}$	closed interval between a and b
$(a, b) \coloneqq \{x \in \mathbb{R} \mid a < x < b\}$	open interval between a and b
$[a, b) \coloneqq \{x \in \mathbb{R} \mid a \leq x < b\}$	half-open interval between a and b
$\hbar$	reduced Planck constant (set equal to unity, unless mentioned otherwise)
$\mathcal{H}_j$	local Hilbert space at site $j \in \Lambda$
$\mathcal{H} \coloneqq \bigotimes_j \mathcal{H}_j$	entire Hilbert space of the quantum system
$\mathrm{Span}\{\lvert\psi\rangle \in \mathcal{H} \mid \mathscr{C}\}$	Hilbert subspace spanned by $\lvert\psi\rangle$ that satisfy the condition $\mathscr{C}$
$\mathrm{End}\,\mathcal{H}$	set of endomorphisms or linear operators on $\mathcal{H}$
$\mathrm{Ker}\,P$	kernel of linear operator P
σ_j^α $(\alpha = x, y, z)$	Pauli matrix at site j
S	spin quantum number (for given S, $\dim \mathcal{H}_j = 2S + 1$)

Acronyms

AKLT	Affleck-Kennedy-Lieb-Tasaki
EE	Entanglement Entropy
ETH	Eigenstate Thermalization Hypothesis
GOE	Gaussian Orthogonal Ensemble
LIOM	Local Integrals Of Motion
MBL	Many-Body Localization/Localized
MPO	Matrix Product Operator
MPS	Matrix Product State
OBC	Open Boundary Condition
PBC	Periodic Boundary Condition
QMBS	Quantum Many-Body Scar/Scarred
RSGA	Restricted Spectrum Generating Algebra
SGA	Spectrum Generating Algebra

Table of Contents

List of Tables

List of Figures

"To be, or not to be, that is the question."
– William Shakespeare, *Hamlet*

CHAPTER 1

INTRODUCTION

Thermalization is such a ubiquitous phenomenon in macroscopic systems that we observe it every day. However, understanding its origin at the microscopic level, or from quantum mechanics, is far from established yet in spite of a long history of research [1, 2]. Recent progress in quantum engineering enabled us to tackle this long-standing problem experimentally. For instance, several experimental groups directly observed thermalization in quantum many-body systems including ultracold atoms [3] and superconducting qubits [4]. On the other hand, surprisingly, experimentalists also revealed non-thermal behavior with, e.g., Bose gases [5–7], trapped ions [8], and Rydberg atoms [9].

On the theoretical side, both analytical and numerical studies have been devoted to explaining thermalization in quantum many-body systems. For example, several numerical studies [2, 10–12] have captured thermalization in quantum many-body systems. As an analytical approach, several studies have revealed a plausible scenario, namely, the eigenstate thermalization hypothesis (ETH) [13–16]. In this Chapter, after presenting preliminaries, we review ETH and several counterexamples to it. The main topic of the thesis, quantum many-body scars (QMBS), is one of such counterexamples and will be reviewed in detail in Chapter 2.

1.1 Preliminaries

1.1.1 Typicality

Theoretical approaches to explaining macroscopic behavior from the underlying microscopic dynamics date back to Boltzmann [17]. While his studies were based on classical mechanics, von Neumann carried this problem into quantum mechanics [18]. In 1929,

he has already mentioned the concept that is now referred to as *typicality* [19–23]. Although there are several variants to formulate typicality, here we refer to the typicality statement by Refs. [14, 22]. Before doing so, we define our notations as follows:

- $\mathcal{H}$: entire Hilbert space of a quantum system under consideration.
- $H \in \mathrm{End}(\mathcal{H})$: Hamiltonian on $\mathcal{H}$.
- $|E_j\rangle$: normalized energy eigenstate of H with energy eigenvalue E_j, i.e., $H|E_j\rangle = E_j|E_j\rangle$.
- $\mathcal{H}_{[E-\Delta E,E)} \coloneqq \mathrm{Span}\{|E_j\rangle \in \mathcal{H} \mid E_j \in [E-\Delta E, E)\}$: Hilbert subspace of $\mathcal{H}$ called an *energy shell* with energy E and small energy width ΔE.
- $D_{[E-\Delta E,E)} \coloneqq \dim \mathcal{H}_{[E-\Delta E,E)}$: dimension of the energy shell determined by $[E-\Delta E, E)$.
- $\rho^{(\mathrm{mc})}_{[E-\Delta E,E)} \coloneqq P(\mathcal{H}_{[E-\Delta E,E)})/\dim \mathcal{H}_{[E-\Delta E,E)}$: microcanonical ensemble with energy E and energy width ΔE, where $P(\mathcal{H}_{[E-\Delta E,E)})$ is a projector onto $\mathcal{H}_{[E-\Delta E,E)}$.

Let us consider a normalized pure state $|\psi\rangle \in \mathcal{H}_{[E-\Delta E,E)}$ drawn from the uniform distribution on $\mathcal{H}_{[E-\Delta E,E)}$. To be more precise, when $|\psi\rangle$ is written as a linear combination of energy eigenstates

$$|\psi\rangle = \sum_{\substack{j \\ E_j \in [E-\Delta E,E)}} c_j |E_j\rangle, \tag{1.1}$$

the coefficients $\{c_j\}$ are chosen from the uniform distribution on the surface of the sphere defined by

$$\sum_{\substack{j \\ E_j \in [E-\Delta E,E)}} |c_j|^2 = 1. \tag{1.2}$$

We denote by $\mu[\mathscr{C}]$ the probability of obtaining $|\psi\rangle$ satisfying the statement $\mathscr{C}$ under the above measure. Then, one can prove that [14, 22]

$$\mu\left[\left|\langle\psi|O|\psi\rangle - \mathrm{tr}\left(O\rho^{(\mathrm{mc})}_{[E-\Delta E,E)}\right)\right| \geq \varepsilon\right] \leq \frac{\|O\|^2}{\varepsilon^2 D_{[E-\Delta E,E)}}, \tag{1.3}$$

or roughly,

$$\langle\psi|O|\psi\rangle \simeq \mathrm{tr}\left(O\rho^{(\mathrm{mc})}_{[E-\Delta E,E)}\right) \tag{1.4}$$

holds for an arbitrary bounded operator O. Here, $\|\cdot\|$ is the operator norm defined as

$$\|O\| \coloneqq \sup_{\substack{|\psi\rangle \in \mathcal{H} \\ \langle\psi|\psi\rangle = 1}} \sqrt{\langle\psi|O^\dagger O|\psi\rangle}. \tag{1.5}$$

Thus, roughly speaking, typicality implies that almost all pure states are indistinguishable from the microcanonical ensemble as long as we look at the expectation value of O.

One may think that thermalization is obvious from typicality, but it is not the case. In a realistic experimental setup, we start with a very atypical initial state and observe its quench dynamics. However, one cannot claim from typicality that an atypical initial state becomes thermalized after a sufficiently long time [24]. In fact, it is known that, in several systems discussed below, the expectation value of an observable for an evolved pure state $|\psi(t)\rangle \coloneqq \mathrm{e}^{-\mathrm{i}Ht}\,|\psi(0)\rangle$ does not converge to that for the microcanonical ensemble for a long time even if we choose an atypical but simple initial state $|\psi(0)\rangle$ [25]. To summarize, typicality does not explain either the dynamics toward equilibrium or the reason why a state eventually becomes thermalized in many systems but does not in several exceptional systems.

1.1.2 Equilibration and thermalization

To understand the dynamics toward equilibrium, let us consider the simplest situation. We assume that each energy of the Hamiltonian H is not degenerate. For a generic initial state $|\psi(t=0)\rangle = \sum_j c_j\,|E_j\rangle$, the long-time average of the expectation value of an observable O can be computed as

$$\lim_{T\to\infty}\frac{1}{T}\int_0^T \langle O\rangle_t\,dt \coloneqq \lim_{T\to\infty}\frac{1}{T}\int_0^T \langle\psi(t)|\,O\,|\psi(t)\rangle\;dt = \sum_j |c_j|^2\,\langle E_j|\,O\,|E_j\rangle\,. \tag{1.6}$$

Here, we explicitly use the assumption that $E_j \neq E_k$ for $j \neq k$. This value equals the expectation value for the time-averaged density matrix, or the diagonal ensemble [10, 26], defined as

$$\rho_{\mathrm{DE}} \coloneqq \lim_{T\to\infty}\frac{1}{T}\int_0^T |\psi(t)\rangle\,\langle\psi(t)|\;dt = \sum_j |c_j|^2\,|E_j\rangle\,\langle E_j|\,. \tag{1.7}$$

In other words, the time-averaged expectation value of any observable for an arbitrary initial state converges to its diagonal ensemble expectation value

$$\langle O\rangle_{\mathrm{DE}} \coloneqq \mathrm{tr}(O\rho_{\mathrm{DE}}) = \sum_j |c_j|^2\,\langle E_j|\,O\,|E_j\rangle\,. \tag{1.8}$$

Thus, we can define a *temporal fluctuation* of an observable O as $|\langle O\rangle_t - \langle O\rangle_{\mathrm{DE}}|$. If the temporal fluctuation is small enough, we can conclude that $\langle O\rangle_t$ converges, and thus the system equilibrates. One can obtain the following upper bound on the temporal fluctua-

tion [27] under an additional assumption called the non-resonance condition[1] [13, 14]:

$$\lim_{T\to\infty}\frac{1}{T}\int_0^T |\langle O\rangle_t - \langle O\rangle_{\mathrm{DE}}|^2\, dt \le \frac{\|O\|^2}{D_{\mathrm{eff}}}. \tag{1.10}$$

Here, D_{eff} is called the effective dimension defined as

$$D_{\mathrm{eff}} \coloneqq \frac{1}{\sum_j |c_j|^4}. \tag{1.11}$$

It is easily verified that $1 \le D_{\mathrm{eff}} \le \dim \mathcal{H}$, and, roughly speaking, D_{eff} represents the effective number of energy eigenstates that contribute to the initial state. Inequality (1.10) ensures the relaxation to equilibrium if D_{eff} of the initial state is sufficiently large, which is typically true [14].

We have seen equilibration of $\langle O\rangle_t$ under rather realistic assumptions. However, this is not the end of the story because the equilibrium value $\langle O\rangle_{\mathrm{DE}}$ does not necessarily agree with the thermal equilibrium value computed with a microcanonical ensemble. In other words, we need to distinguish equilibration from thermalization [28]. The former means that the time-averaged $\langle O\rangle_t$ reaches a constant value (up to small temporal fluctuations) and has been proved in a rather generic setup. On the other hand, the latter means that the time-averaged $\langle O\rangle_t$ coincides with the expectation value for a microcanonical ensemble with energy $\langle\psi(0)|\, H\, |\psi(0)\rangle$. Then, a natural question is: what are necessary or sufficient conditions for systems to thermalize? As seen in Sec. 1.2, the (strong) ETH is a sufficient condition for thermalization of isolated quantum systems.

1.2 Eigenstate Thermalization Hypothesis

Let us now introduce the ETH, a plausible scenario to explain thermalization in isolated quantum systems. For simplicity, we consider lattice systems such as quantum spin models and the Hubbard model. There are two types of ETH, namely, the strong ETH and the weak ETH. The strong ETH states that *all* energy eigenstates are locally indistinguishable from the microcanonical ensemble [13, 14, 29–31]:

$$\langle E_j|\, O\, |E_j\rangle \simeq \mathrm{tr}\left(O\rho^{(\mathrm{mc})}_{[E-\Delta E,E)}\right) \quad \text{for all } |E_j\rangle \in \mathcal{H}_{[E-\Delta E,E)}, \tag{1.12}$$

or more precisely [32],

$$\max_{\substack{j\\ e_1\le E_j/V\le e_2}} \left|\left\langle E_j^{(V)}\right| O \left|E_j^{(V)}\right\rangle - \mathrm{tr}\left(O\rho^{(\mathrm{mc}),(V)}_{[E-\Delta E,E)}\right)\right| \xrightarrow{V\to\infty} 0. \tag{1.13}$$

[1] The condition imposes no degeneracy of *energy gaps*: for any k,l,m,n,

$$E_k - E_l = E_m - E_n \iff (k=l\ \&\ m=n) \ \text{ or } \ (k=m\ \&\ l=n). \tag{1.9}$$

Here, O is any density of local and macroscopic operator, V is the number of lattice sites, and $\left|E_j^{(V)}\right\rangle$ and $\rho_{[E-\Delta E,E)}^{(\mathrm{mc}),(V)}$ are an energy eigenstate and the density operator of a microcanonical ensemble with V, respectively. The condition for the energy density, $e_1 \leq E_j/V \leq e_2$, should be taken in the middle of the energy spectrum, since some peculiar behaviors may occur for the ground state or low-lying excited states (see also the footnote of the definition of QMBS in Sec. 2.1.1). Note that Eq. (1.12) is different from Eq. (1.4); the former is the condition for energy eigenstates, whereas the latter is for a randomly chosen state from $\mathcal{H}_{[E-\Delta E,E)}$. Although there is no rigorous proof of the strong ETH, it is widely believed to hold for a large class of interacting systems, as evidenced by several numerical studies [2, 10–12]. On the other hand, the weak ETH states that *almost all* energy eigenstates are locally indistinguishable from the microcanonical ensemble [14–16, 31], or more precisely, for any $\varepsilon > 0$,

$$\mathrm{Prob}_{\mathcal{H}_{[E-\Delta E,E)}}\left[\left|\left\langle E_j^{(V)}\right| O \left|E_j^{(V)}\right\rangle - \mathrm{tr}\left(O\rho_{[E-\Delta E,E)}^{(\mathrm{mc}),(V)}\right)\right| > \varepsilon\right] \xrightarrow{V\to\infty} 0. \tag{1.14}$$

Here, we introduce a notation $\mathrm{Prob}_{\mathcal{H}_{[E-\Delta E,E)}}[\mathscr{C}] := n_{\mathrm{true}}[\mathscr{C}]/\dim \mathcal{H}_{[E-\Delta E,E)}$ as a "probability"[2] that statement $\mathscr{C}$ is true with respect to the uniform distribution on $|E_j\rangle \in \mathcal{H}_{[E-\Delta E,E)}$, where $n_{\mathrm{true}}[\mathscr{C}]$ is the number of energy eigenstates $|E_j\rangle \in \mathcal{H}_{[E-\Delta E,E)}$ which satisfy $\mathscr{C}$. Note that the weak ETH allows the existence of athermal states, although the number of them should be much smaller than that of thermal states. The weak ETH was proved for generic translationally invariant short-range interacting systems [16].

Now, let us see that thermalization of an isolated quantum system can be shown when the strong ETH holds. Eqs. (1.8) and (1.12) leads to

$$\mathrm{tr}\left(O\rho_{[E-\Delta E,E)}^{(\mathrm{mc})}\right) \simeq \langle O\rangle_{\mathrm{DE}}. \tag{1.15}$$

We have also seen that the time-averaged $\langle O\rangle_t$ converges to $\langle O\rangle_{\mathrm{DE}}$. Therefore, we conclude that the time-averaged $\langle O\rangle_t$ agrees with $\mathrm{tr}\left(O\rho_{[E-\Delta E,E)}^{(\mathrm{mc})}\right)$, which is the definition of thermalization.

However, it is known that several systems to be discussed below do not thermalize, which implies that the strong ETH does not hold for all systems. Moreover, some systems violate the weak ETH as well. While there are two types of violation, namely, violation of the strong ETH and that of the weak ETH, in this thesis, we use "violation of the ETH" in the sense of that of the strong ETH, unless otherwise stated.

[2] We use these terminology and notation according to several papers [16, 31], but we are afraid that the terminology is confusing, and thus some care has to be taken. Here, "probability" does not mean the probability with respect to the uniform distribution on $\mathcal{H}_{[E-\Delta E,E)}$, as discussed in Sec. 1.1.1. Instead, we just check if statement $\mathscr{C}$ is true for each of $\{|E_j\rangle \mid E_j \in [E-\Delta E, E)\}$, which is just a (countable) set of vectors and not the Hilbert subspace $\mathcal{H}_{[E-\Delta E,E)} = \mathrm{Span}\{|E_j\rangle \mid E_j \in [E-\Delta E, E)\}$. We then define $\mathrm{Prob}_{\mathcal{H}_{[E-\Delta E,E)}}[\mathscr{C}]$ as the ratio of $n_{\mathrm{true}}[\mathscr{C}]$ to $D_{[E-\Delta E,E)} = |\{|E_j\rangle \mid E_j \in [E-\Delta E, E)\}|$. It is important to note that, when some energy levels are degenerate, $n_{\mathrm{true}}[\mathscr{C}]$ may depend on the choice of orthogonal eigenstates $\{|E_j\rangle\}$.

1.3 Violation of ETH

In this section, let us see several counterexamples to the ETH, namely, integrable systems, many-body localized (MBL) systems, and systems with Hilbert space fragmentation. While a QMBS system is also a counterexample to the ETH, it will be defined in Chapter 2 as their complement, i.e., as an ETH-violating system that is not integrable, many-body localized, or fragmented.

1.3.1 Integrable systems

Roughly speaking, the ETH violation in integrable systems can be understood as follows. In an integrable system, there are an extensive number (typically $\mathcal{O}(L)$ for the system size L) of conserved quantities [33], which means that a state at any time $t > 0$ remembers information at time $t = 0$ forever. On the other hand, we expect that thermal equilibrium does not depend on the details of the initial states but only on a small number of local and macroscopic conserved quantities such as the total energy and the number of particles. This discrepancy implies the lack of thermalization in integrable systems.

The above discussion might be naive and phenomenological, but several studies [11, 25, 26, 34–37] indeed revealed an atypical behavior in integrable systems. Here, let us review Ref. [37] as a pedagogical example. The authors in Ref. [37] studied the one-dimensional XXZ model in one dimension with/without next-nearest neighbor hopping and interactions described by the following Hamiltonian:

$$H_{\mathrm{XXZ}} \coloneqq \frac{1}{1+\lambda}(H_0 + \lambda W), \tag{1.16}$$

$$H_0 \coloneqq \sum_{j=1}^{L} \left(-b_j^\dagger b_{j+1} - b_j b_{j+1}^\dagger + n_j n_{j+1}\right), \tag{1.17}$$

$$W \coloneqq \sum_{j=1}^{L} \left(-b_j^\dagger b_{j+2} - b_j b_{j+2}^\dagger + n_j n_{j+2}\right). \tag{1.18}$$

Here, $b_j^\dagger$ and b_j are creation and annihilation operators of hard-core bosons, satisfying

$$[b_j, b_k^\dagger] = [b_j, b_k] = [b_j^\dagger, b_k^\dagger] = 0 \quad (j \neq k), \tag{1.19}$$

$$\{b_j, b_j^\dagger\} = 1,\ (b_j)^2 = (b_j^\dagger)^2 = 0, \tag{1.20}$$

L is the number of sites, and we impose the periodic boundary condition (PBC), i.e., $b_{L+1} = b_1,\ b_{L+2} = b_2$, hence translational invariance. The original XXZ chain described by H_0 is a well-known integrable model, which can be solved by the Bethe ansatz [38, 39]. The next-nearest neighbor hopping and interaction term W, however, breaks the integrability of the system, so $\lambda \geq 0$ can be interpreted as a degree of integrability breaking. Then, they

investigated the scaling of

$$D_{\mathrm{out}}/D \coloneqq \mathrm{Prob}_{\mathcal{H}_{[E-\Delta E,E)}}\left[\left|\langle E_j|\,O\,|E_j\rangle - \mathrm{tr}\left(O\rho^{(\mathrm{mc})}_{[E-\Delta E,E)}\right)\right| > \varepsilon\right],$$

with respect to the system size L for various λ and a certain O. In our notations, D_{out} and D are defined as

$$D_{\mathrm{out}} \coloneqq n_{\mathrm{true}}\left[\left|\langle E_j|\,O\,|E_j\rangle - \mathrm{tr}\left(O\rho^{(\mathrm{mc})}_{[E-\Delta E,E)}\right)\right| > \varepsilon\right]$$

and

$$D \coloneqq \dim \mathcal{H}_{[E-\Delta E,E)},$$

respectively. They found that

1. when $\lambda = 0$, D_{out}/D decays exponentially, but the number of those athermal states D_{out} increases exponentially.

2. when $\lambda > 0$, D_{out}/D seems to decay double-exponentially. It suggests that $D_{\mathrm{out}} = 0$ for sufficiently large L since D grows just exponentially.

Their results imply that non-integrable systems obey the strong ETH, but integrable ones do not. On the other hand, the weak ETH is valid for both integrable and non-integrable systems, which is consistent with the proof of the weak ETH with translational invariance [15, 16, 31].

Breakdown of thermalization in nearly integrable systems is also observed experimentally. In Ref. [5], the authors observed the dynamics of a trapped one-dimensional Bose gas, which can be described as a Tonks–Girardeau gas [40, 41], a hard-core limit $c \to \infty$ of the Lieb-Liniger model [42, 43] with the Hamiltonian

$$H_{\mathrm{LL}} \coloneqq -\frac{1}{2m}\sum_{j=1}^{N}\frac{\partial^2}{\partial x_j^2} + 2c\sum_{1\le j<k\le N}\delta(x_j - x_k), \tag{1.21}$$

in the anharmonic trap (see also Fig. 1.1). Here, N is the number of bosons. The system was initially prepared in a momentum superposition with $\pm 2\hbar k$, where k is the wavevector of the 1D lattice light. Then, they monitored the spatial distribution of a Bose gas and observed its robust oscillations for a long time. This atypical behavior illustrated the experimental realization of a Lieb-Liniger model with pointlike interactions and the absence of thermalization in a nearly integrable system. They called the experiment a quantum Newton's cradle since it is reminiscent of a classical one as illustrated in Fig. 1.1.

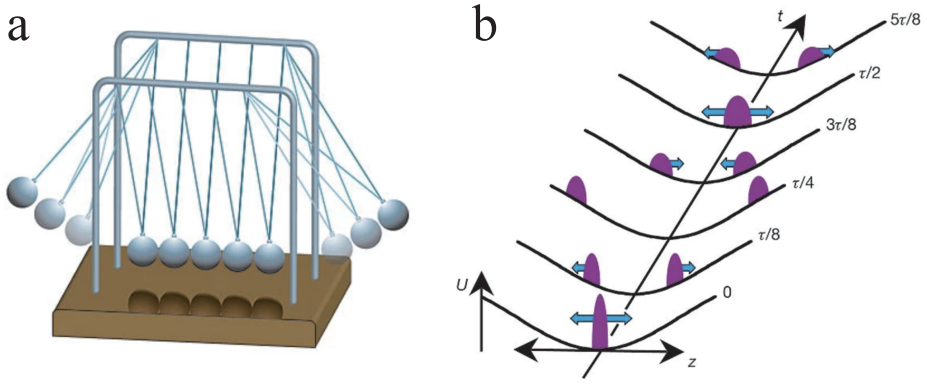

Figure 1.1: **a.** Classical and **b.** quantum Newton's cradles. Figure **b.** represents the schematic dynamics of the clouds of atoms in a 1D anharmonic trap. Figures reproduced with permission from Ref. [5], Springer Nature Ltd.

1.3.2 Many-body localized systems

As mentioned above, the weak ETH is proved for generic translationally invariant short-range interacting systems. Then, it is a natural question to ask whether the ETH holds in the absence of translational invariance.

Systems in the presence of strong disorder can exhibit *localization*, which was first proposed by Anderson [44]. Although Anderson originally studied single-particle localization, such localization can occur even in interacting systems, which is now referred to as *many-body localization* (MBL) [45–48]. The spin-$1/2$ Heisenberg chain in a random magnetic field[3] with the Hamiltonian [45, 50, 51]

$$H_{\mathrm{rfH}} \coloneqq \sum_j \left(S_j^x S_{j+1}^x + S_j^y S_{j+1}^y + S_j^z S_{j+1}^z + h_j S_j^z \right) \tag{1.22}$$

is a prototypical example of MBL systems. Here, h_j are independent random variables from a uniform distribution on $[-h, h]$, and h is a disorder strength. Extensive numerical studies [45, 50, 51] captured the MBL transition at the critical disorder strength $h = h_{\mathrm{c}}$ and the violation of the weak ETH in the MBL phase. Here, let us see how to characterize the MBL phase and why the MBL system fails to thermalize.

Level-spacing statistics have been frequently used to distinguish non-integrable systems from integrable ones, and it can also be used to differentiate extended and localized phases. Let $E_0 \leq E_1 \leq \cdots \leq E_j \leq \ldots$ be energy levels in ascending order, $\Delta E_j \coloneqq E_{j+1} - E_j$ gaps between the consecutive energy levels, and $\langle \Delta E \rangle$ an average of ΔE_j, i.e.,

$$\langle \Delta E \rangle \coloneqq \frac{1}{\mathscr{N}} \sum_{j=0}^{\mathscr{N}-1} \Delta E_j,$$

[3] The model is equivalent to that of interacting spinless fermions with the random chemical potential [49] via the Jordan-Wigner transformation.

where $\mathscr{N}$ is the number of ΔE_j's. It is known [52–55] that the normalized energy-level spacings $s_j \coloneqq \Delta E_j / \langle \Delta E \rangle$ obey the Wigner-Dyson distribution with the probability density function

$$P_{\mathrm{WD}}(s) \coloneqq \frac{\pi}{2} s \mathrm{e}^{-\pi s^2/4} \tag{1.23}$$

for chaotic systems described by the random matrix theory of the Gaussian orthogonal ensemble (GOE), and the Poisson distribution with the probability function

$$P_{\mathrm{P}}(s) \coloneqq \mathrm{e}^{-s} \tag{1.24}$$

for integrable systems. The ratio of adjacent level spacings (also known as the r value) [56, 57]

$$\langle r \rangle \coloneqq \left\langle \frac{\min(\Delta E_j, \Delta E_{j+1})}{\max(\Delta E_j, \Delta E_{j+1})} \right\rangle = \frac{1}{\mathscr{N}-1} \sum_{j=0}^{\mathscr{N}-2} \frac{\min(\Delta E_j, \Delta E_{j+1})}{\max(\Delta E_j, \Delta E_{j+1})} \tag{1.25}$$

is often used for quantitative detection of distribution statistics; $\langle r \rangle_{\mathrm{WD}} = 4 - 2\sqrt{3} \simeq 0.536...$ for the Wigner-Dyson distribution, and $\langle r \rangle_{\mathrm{P}} = 2 \ln 2 - 1 \simeq 0.386$ for the Poisson distribution. In Refs. [45, 51], they found that $\langle r \rangle$ is close to $\langle r \rangle_{\mathrm{WD}}$ when h is small enough and changes toward $\langle r \rangle_{\mathrm{P}}$ as h increases[4], which suggests the transition of level statistics. The similarity between the level statistics of integrable systems and that of strongly disordered systems are apparently surprising. On one hand, integrable systems are in general *fine-tuned* and not robust to any small perturbations. On the other hand, strongly disordered systems apparently seem *chaotic* with a random external field.

Another characteristic of the MBL phase is anomalously low *entanglement entropy* (EE), which measures quantum entanglement. The von Neumann EE of a normalized state $|\phi\rangle$ with respect to a bipartition of the system into subsystems A and $\bar{A}$ is defined as

$$\mathcal{S}_A \coloneqq -\operatorname{tr}(\rho_A \ln \rho_A), \tag{1.26}$$

where $\rho_A \coloneqq \operatorname{tr}_{\bar{A}} |\phi\rangle \langle\phi|$ is a reduced density matrix of region A. We expect that thermal states should have the volume-law EE (with the size of subsystem A), since $\mathcal{S}_A$ essentially corresponds to the thermodynamic entropy of subsystem A [14]. In Ref. [51], they compared the averaged EE of highly excited eigenstates in the extended phase with that in the MBL phase and found quantitative differences of the EE scalings between the two phases: the volume-law scaling for the extended phase and the area-law scaling for the MBL phase. Their results imply that even the weak ETH is violated in the MBL phase since the EE is averaged over different highly excited eigenstates.

[4] The model is integrable when h is exactly 0, and will not show the Wigner-Dyson distribution. Thus, here we consider small but nonzero h in an extended phase.

The reason why MBL systems fail to thermalize is in fact similar to that for integrable systems: there are an extensive number of *local integrals of motions* (LIOMs). They were first phenomenologically introduced [58, 59] and shortly afterward constructed rigorously for the random transverse field and random exchange Ising model [60, 61]. Here, we outline the main idea of LIOMs. We expect that the Hamiltonian in the MBL phase can be rewritten in terms of localized pseudospins $\{\boldsymbol{\tau}_j\}$ as

$$H = E_0 + \sum_j \tau_j^z + \sum_{j,k} J_{j,k}\tau_j^z\tau_k^z + \sum_{j,k,l} J_{j,k,l}\tau_j^z\tau_k^z\tau_l^z + \cdots, \tag{1.27}$$

and a localized pseudospin τ_j^z at site j is constructed only by neighboring spins:

$$\tau_j^z = \sigma_j^z + \sum_{k,l} \sum_{\alpha,\beta=x,y,z} c_{j,k,l}^{\alpha,\beta}\sigma_k^\alpha\sigma_l^\beta + \cdots. \tag{1.28}$$

Here, $\sigma_k^\alpha \coloneqq 2S_k^\alpha$ is a standard Pauli matrix at site k, and interaction strength $J_{j,k,l,\ldots}$ between pseudospins and coefficients c are expected to decay exponentially with the distance between site j and other sites. Note that the phenomenological Hamiltonian (1.27) is *classical*, i.e., only consists of τ_j^z; however, τ_j^x and τ_j^y never appear. Thus the Hamiltonian is diagonalized by the set of eigenvalues ± 1 for each LIOM τ_j^z. The intuition behind Eq. (1.27) is that the Hamiltonian should be written in terms of such localized conserved charges $\{\tau_j^z\}$ since there is no transport in the fully localized regime [59]. From this phenomenological view, one can see that the existence of LIOMs yields a long-time memory of the initial state, which results in the lack of thermalization.

Finally, we briefly review experiments on MBL. The first experimental observation of MBL was carried out in one-dimensional interacting ultracold fermions in a quasi-random optical lattice [62], which can be described by the Hamiltonian

$$H = -J\sum_{j,\sigma}(c_j^\dagger c_{j+1} + \text{h.c.}) + \Delta\sum_{j,\sigma}\cos(2\pi\beta j + \phi)n_{j,\sigma} + U\sum_j n_{j,\uparrow}n_{j,\downarrow}. \tag{1.29}$$

Here, $c_j^\dagger$ and c_j are creation and annihilation operators for fermions at site j with spin state $\sigma = \uparrow, \downarrow$, $n_{j,\sigma} \coloneqq c_{j,\sigma}^\dagger c_{j,\sigma}$ is the number operator at site j, J is the tunneling amplitude between neighboring lattice sites, β is the ratio of lattice periodicities, ϕ is phase offset, Δ is disorder strength, and U is the onsite interaction energy. They measured the imbalance between the number of atoms on even (N_e) and odd (N_o) sites

$$\mathcal{I} \coloneqq \frac{N_\mathrm{e} - N_\mathrm{o}}{N_\mathrm{e} + N_\mathrm{o}}. \tag{1.30}$$

In the initial state, all atoms were placed only on even sites, so $\mathcal{I} \simeq 1$. When disorder strength Δ is small enough, $\mathcal{I}$ quickly relaxed to zero. On the other hand, for stronger disorder, it remained a nonzero stationary value for a long time, which implies that the system keeps a memory of the initial state.

Another experiment was reported in Ref. [8]. Using trapped $^{171}\mathrm{Yb}^{+}$ ions, they experimentally investigated a long-range transverse field Ising model with disorder described by the Hamiltonian

$$H = \sum_{j<k} J_{j,k}\sigma_j^x\sigma_k^x + \frac{B}{2}\sum_j \sigma_j^z + \sum_j \frac{D_j}{2}\sigma_j^z. \tag{1.31}$$

Here, $\sigma_j^{x,z}$ are the Pauli matrices at site j, $J_{j,k}$ is the coupling strength between spins at sites j and k, B is a uniform effective transverse field, and D_j is a site-dependent random transverse field. The coupling $J_{j,k}$ is tuned to decay algebraically as $J_{j,k} \propto J_{\max}/|j-k|^{\alpha}$ with $J_{\max} \simeq 2\pi$ and $\alpha \simeq 1.13$. The random transverse field D_j can also be tuned and were randomly sampled from a uniform distribution on $[-W, W]$, with disorder strength W. Preparing the Néel state $|\psi_0\rangle = |\uparrow\downarrow\uparrow\downarrow\ldots\rangle$ along the z direction as the initial state, they measured the time evolution of expectation value $\langle\sigma_j^z\rangle$ and the (normalized) Hamming distance

$$\mathcal{D}(t) := \frac{1}{2} - \frac{1}{2L}\sum_j \langle\psi_0|\,\sigma_j^z(t)\sigma_j^z(0)\,|\psi_0\rangle\,, \tag{1.32}$$

which is, roughly speaking, the proportion of flipped spins at time t. They observed thermal/athermal behaviors in the absence/presence of disorder:

- $\langle\sigma_j\rangle$ decays quickly to zero without disorder, while it keeps a non-vanishing value for a long time with stronger W.
- $\mathcal{D}(t)$ reaches to 0.5 in the absence of disorder. On the other hand, it becomes smaller even for a long time as W is increased.

These results clearly capture the features of MBL and agree well with the theoretical prediction.

1.3.3 Hilbert space fragmentation

The above two counterexamples to the ETH, integrable systems and MBL systems, have local conserved quantities or integrals of motions, which essentially cause the lack of ergodicity[5]. Other systems can exhibit non-ergodic behaviors due to the *Hilbert space fragmentation* into exponentially many disconnected sectors that cannot be labeled by local quantities. One of such examples is the one-dimensional t-J_z model described by the Hamiltonian [63–65] with the open boundary condition (OBC)

$$H_{t\text{-}J_z} := -t\sum_{\substack{j=1\\ \sigma=\uparrow,\downarrow}}^{L-1}\left(\tilde{c}_{j,\sigma}\tilde{c}_{j+1,\sigma}^{\dagger} + \tilde{c}_{j+1,\sigma}\tilde{c}_{j,\sigma}^{\dagger}\right) + J_z\sum_{j=1}^{L-1} S_j^z S_{j+1}^z, \tag{1.33}$$

[5]The notion of ergodicity in quantum mechanics is not as clear as in classical mechanics [1, 18]. However, here we roughly mean by ergodicity that the system forgets the details of the initial state.

with the number of sites L. Here, $\tilde{c}_{j,\sigma}$ are dressed fermionic operators with the hard-core constraint and can be written with standard fermionic operators $c_{j,\sigma}$ as $\tilde{c}_{j,\sigma} \coloneqq c_{j,\sigma}(1 - c^\dagger_{j,-\sigma}c_{j,-\sigma})$. Due to the constraint, the dimension of each local Hilbert space is three. We refer to these three local states as $|0\rangle, |\uparrow\rangle$, and $|\downarrow\rangle$, where 0 stands for the empty site and $\uparrow$ ($\downarrow$) for the site occupied by a fermion with the up-spin (down-spin) index. The spin operator S^z_j can be written in terms of dressed fermions as $S^z_j \coloneqq (\tilde{c}^\dagger_{j,\uparrow}\ \tilde{c}^\dagger_{j,\downarrow})(\sigma^z/2)(\tilde{c}_{j,\uparrow}\ \tilde{c}_{j,\downarrow})^{\mathrm{T}}$, where σ^z is the standard Pauli matrix.

There are two local conserved quantities, namely, the number of fermions $N_{\mathrm{F}} \coloneqq \sum_j (n_{j,\uparrow} + n_{j,\downarrow})$ and the total spin $S^z_{\mathrm{tot}} \coloneqq \sum_j (n_{j,\uparrow} - n_{j,\downarrow})/2$, where $n_{j,\sigma} \coloneqq \tilde{c}^\dagger_{j,\sigma}\tilde{c}_{j,\sigma}$ is the number operator at site j. In addition to these, the model possesses nonlocal conserved quantities. One can see that the sequences of local states from which 0 are omitted remain unchanged[6] due to the hard-core constraint and the absence of $S^x_j S^x_{j+1}$ or $S^y_j S^y_{j+1}$ terms. Thus, the model has the nonlocal conserved quantities defined as

$$q_k \coloneqq \sum_{j=1}^{L} \mathcal{P}^k_j S^z_j, \tag{1.34}$$

where $\mathcal{P}^k_j$ is the projection operator onto the Hilbert subspace where the k-th fermion is exactly on site j. In the case of $k = 1$, it reduces to a simpler form:

$$q_1 = \sum_{j=1}^{L} \left[\prod_{k=1}^{j-1}(1 - n_k)\right] S^z_j. \tag{1.35}$$

These nonlocal conserved quantities make the Hilbert space split into exponentially many disconnected subsectors. To be more precise, for a given N_{F}, there are $2^{N_{\mathrm{F}}}$ distinct subsectors determined by the pattern of $\uparrow$ and $\downarrow$, and thus the total number of connected components is

$$\sum_{N_{\mathrm{F}}=0}^{L} 2^{N_{\mathrm{F}}} = 2^{L+1} - 1. \tag{1.36}$$

Figure 1.2 represents the connectivity of the Hilbert space by interpreting $H_{t\text{-}J_z}$ as an adjacent matrix of the graph, each vertex of which corresponds to the product state of $|0\rangle, |\uparrow\rangle$, and $|\downarrow\rangle$.

Hilbert space fragmentation yields nonergodicity, which leads to a violation of the ETH. Such an atypical behavior is also captured by computing an expectation value. In Ref. [65], they numerically calculated the expectation value of $S^z_{L/2}S_{L/2+1}$ for every eigenstate and expected that the width of its distribution would scale as $L^{-1/4}$. This scaling is even slower than that of integrable systems, which is typically $L^{-1/2}$ [31, 36]. From these results, they concluded the violation of the ETH.

[6] Such a constraint also appears in the one-dimensional infinite-U Hubbard model [66].

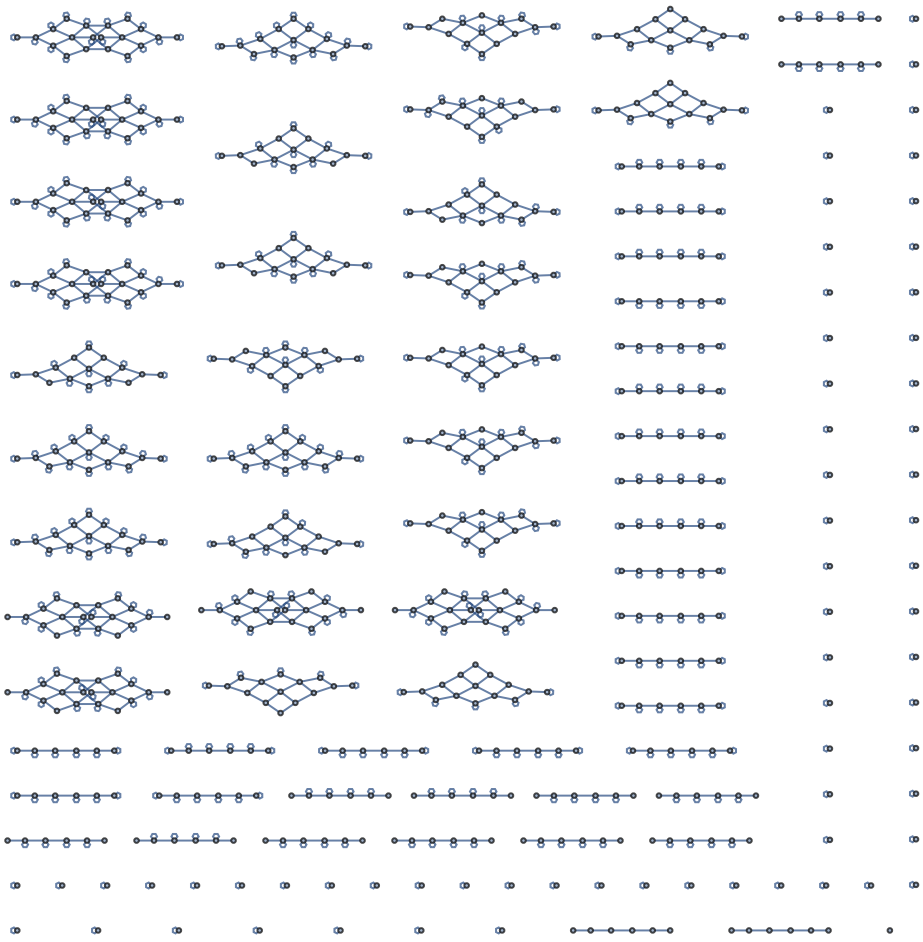

Figure 1.2: A visualization of Hilbert space fragmentation of the $t-J_z$ model with $L = 6$. Each vertex denotes the product state of $|0\rangle, |\uparrow\rangle$, and $|\downarrow\rangle$ such as $|0 \uparrow\uparrow\downarrow 0 \downarrow\rangle$. Since the order of $\uparrow$ and $\downarrow$ does not change, $|0 \uparrow\uparrow\downarrow 0 \downarrow\rangle$ does not connect with, for example, $|0 \uparrow\downarrow\uparrow 0 \downarrow\rangle$. This constraint splits the Hilbert space into $2^{L+1} - 1$ ($= 127$ in the $L = 6$ case) disconnected subsectors.

Another example of Hilbert space fragmentation is the one-dimensional spin-1 dipole-conserving model described by the following Hamiltonian [67] with the OBC:

$$H_3 := -\sum_{j=-l+1}^{l-1} \left[S^+_{j-1}(S^-_j)^2 S^+_{j+1} + S^-_{j-1}(S^+_j)^2 S^-_{j+1} \right]. \tag{1.37}$$

Here, we assume that the number of sites $L = 2l + 1$ is odd and label each site $j = -l, -l+1, \ldots, l-1, l$, and $S^\pm_j$ is a spin raising/lowering operator of $S = 1$ at site j. This model has two local conserved quantities; the $\mathrm{U}(1)$ charge Q and the dipole moment P

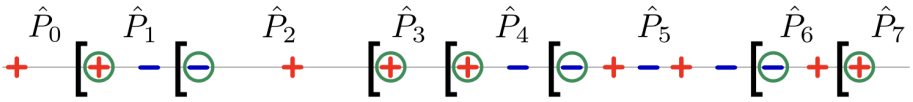

Figure 1.3: Defects and nonlocal conserved quantities of the dipole-conserving model H_3. Green circles denote the defects, the charge sign of which is the same as that of the left one. The total number and pattern of defects are conserved by H_3. In addition, the dipole moment $\hat{P}_k$ within each region (indicated by the brackets) between two subsequent defects is also conserved. Figure reproduced with permission from Ref. [65], American Physical Society.

defined as

$$Q \coloneqq \sum_{j=-l}^{l} S_j^z, \quad P \coloneqq \sum_{j=-l}^{l} j S_j^z. \tag{1.38}$$

Besides these, the number and pattern of *defects* defined below are conserved in this model. Let us denote the S^z basis with eigenvalues $+1$, 0, and -1 as $|+\rangle$, $|0\rangle$, and $|-\rangle$, and refer to them as a positive charge, an empty site, and a negative charge, respectively. Then, a defect is defined as a charge that has the same sign as the one on its left with empty sites ignored (see also Fig. 1.3). Moreover, one can see that the dipole moments within the region between two subsequent defects are also conserved. Due to the existence of such nonlocal conserved quantities, the Hilbert space is fragmented into exponentially many subsectors, which yields several peculiar behaviors such as non-vanishing autocorrelator for a long time, the wide distribution of the eigenstate expectation value, and anomalously low EE of eigenstates [67]. Intriguingly, this model was experimentally realized in the tilted Fermi-Hubbard chain [68], and non-ergodic behaviors were observed directly.

Before finishing this section, we remark the apparent discrepancy between the absence of thermalization in the above systems and the rigorous proof that the weak ETH holds for generic translationally invariant short-range interacting systems. Since we impose the OBC on $H_{t\text{-}J_z}$ and H_3, their translational invariance is not perfect, but we expect that macroscopic behaviors do not depend on boundary conditions. In fact, non-ergodic behavior was also captured under the PBC [65]. Then, one may think that $H_{t\text{-}J_z}$ and H_3 are counterexamples of the proof of the weak ETH. This apparent contradiction stems from the ambiguity of the choice of eigenstates. The Hamiltonians $H_{t\text{-}J_z}$ and H_3 have many exponentially degenerate eigenvalues due to their fragmentation, and thus a set of orthogonal eigenstates is not unique. However, it depends on the choice of eigenstates whether each eigenstate is thermal or not. The rigorous results on the weak ETH [16, 31] claim that there exists a set of orthogonal eigenstates almost all of which are thermal. In general, such eigenstates can be superpositions of states each of which lives in a differ-

ent disconnected subsector. In other words, the proof of the weak ETH, for now, can not rule out the possibility of the existence of anomalously many athermal states when the Hamiltonian has exponentially degenerate eigenstates.

1.4 Summary of the Chapter and Outline of the Thesis

We have briefly reviewed the existence/absence of thermalization in various quantum many-body systems from both theoretical and experimental points of view and introduced the theoretical plausible scenario called the ETH. Although the ETH is believed to be valid in a large class of quantum many-body systems, its violations have been intensively studied theoretically and also observed experimentally. We have focused on the three kinds of counterexamples to the ETH, namely, integrable systems, MBL systems, and systems with Hilbert space fragmentation.

Recently, another distinct class of ETH-violating systems called the *quantum many-body scars* (QMBS) have attracted much attention since the first experimental observation [9]. The initial observation stimulated a number of theoretical studies on QMBS, but its general framework and origin remain unclear. Our motivation is to clarify them and gain a better understanding of QMBS by constructing analytically tractable models.

The organization of the thesis is as follows. In Chapter 2, we review QMBS with several previous works from both theoretical and experimental sides. First, we look through the pioneering experiment performed in Ref. [9] and introduce an effective model as an idealization of the experimental setup. We see that this model has an exact QMBS state written as a matrix product state. Then, we focus on other exact results on QMBS, namely, the systematic construction of QMBS Hamiltonians by embedding athermal states into the middle of the energy spectrum and a particular algebraic structure of scar states appearing in some models, providing their concrete examples.

In Chapter 3, we propose a new construction of exact QMBS models. In particular, we study an $S = 1/2$ spin chain model as the simplest case of our construction. We explicitly write down the exact QMBS states and explain how to construct the QMBS Hamiltonian. We show several numerical results, including the level-spacing statistics, eigenstate expectation values of observables, a half-chain bipartite EE, and dynamics of the fidelity and EE. We also provide an analytical evaluation of EE of QMBS states. All of these results clearly illustrate characteristics of QMBS.

In Chapter 4, we generalize our model constructed in Chapter 3 via the Onsager algebra. First, we briefly review the Onsager algebra and introduce a one-dimensional model that possesses the Onsager symmetry. Then, we provide the generalized construction of our QMBS Hamiltonian to higher spin S or multi-parameter scar states. We also show several numerical results parallel to those in Chapter 3, which demonstrate the validity

of our generalized construction.

Finally, a summary of the thesis is given in Chapter 5. Some supplemental materials are provided in Appendices.

"Scars can come in handy. I have one myself above my left knee that is a perfect map of the London Underground."
– J. K. Rowling, *Harry Potter and the Philosopher's Stone*

CHAPTER 2

QUANTUM MANY-BODY SCARS

In this Chapter, we review quantum many-body scars (QMBS). Before going through its details, let us briefly mention a historical context (see also, e.g., Refs. [69, 70]). According to Ref. [71], the word "scar" seems to have first appeared in Ref. [72], in which Heller studied a quantum analog of the billiard problem. The classical billiard model describes the dynamics of a single particle inside a stadium potential. The collision between the particle and the boundary of the stadium is elastic, so the kinetic energy of the particle is conserved. It was proved [73] that, for a large class of stadium shapes, including the Bunimovich stadium consisting of a rectangle and capped two semicircles, the motion of the particle is almost surely ergodic, i.e., the averaged distribution of the particle for a long enough time is uniform over the whole stadium. However, there also exist non-ergodic and periodic trajectories, although the measure of such trajectories is zero. In Ref. [72], Heller investigated the quantum version of the billiard problem and found that certain eigenfunctions have an imprint of the classical periodic trajectories. To be precise, the wave function of a scarred state concentrates around a classical periodic trajectory (see also Fig. 2.1). He called this imprint of the classical periodic trajectory "scar".

While Ref. [72] studied the one-body quantum system, it is a natural question to ask whether generalization of quantum scars to many-body interacting systems is possible or not. It took over 30 years until the pioneering experiment in the Rydberg atom system [9] revealed the validity of such generalization. We then start this Chapter with this experiment and its effective model.

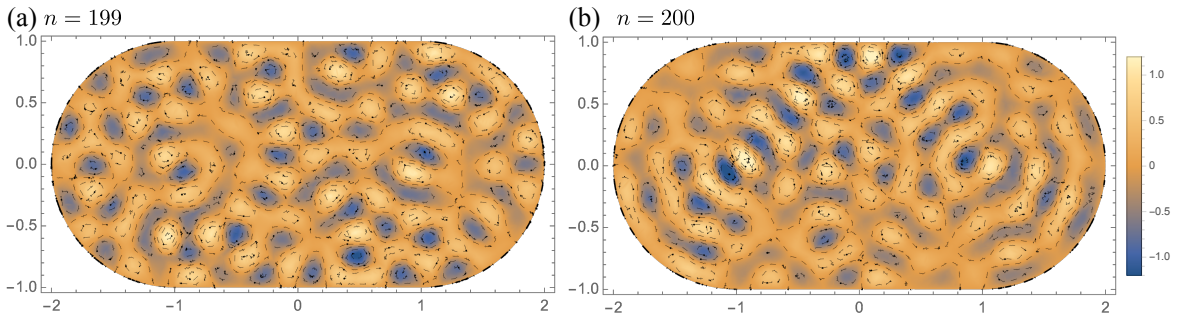

Figure 2.1: Eigenstate wavefunctions with the n-th smallest energy inside the Bunimovich stadium defined as a union of the square $-1 \leq x \leq 1, -1 \leq y \leq 1$ and the two semi-circles $(x-1)^2 + y^2 \leq 1$ $(x \geq 1)$ and $(x+1)^2 + y^2 \leq 1$ $(x \leq -1)$. Here, the x (y)-axis is a horizontal (vertical) one, and we impose the Dirichlet boundary condition that makes wavefunctions vanish at the boundary. Dashed lines indicate contours of the wave functions. For (a) $n = 199$ (or other typical highly excited eigenstates), the wavefunction looks complicated, whereas, for (b) $n = 200$, the wavefunction looks much "simpler" and has a high amplitude around the classical periodic trajectory. Heller called such simple wavefunctions "scars" from the classical periodic trajectory.

2.1 Experiment and Effective Model

2.1.1 First experimental observation

The quantum many-body scars were first observed by Lukin's group in the Rydberg atom system [9], in which cold neutral $^{87}\mathrm{Rb}$ atoms were arranged into arrays and their dynamics were governed by the Hamiltonian

$$H_{\mathrm{Ryd}} \coloneqq \frac{\Omega}{2} \sum_j \sigma_j^x + \sum_{j<k} V_{jk} n_j n_k. \tag{2.1}$$

Here, each atom can be seen as an effective two-level system with the ground state $|g\rangle$ and the Rydberg state $|r\rangle$. The Pauli matrix $\sigma_j^x \coloneqq |g\rangle_j \langle r| + |r\rangle_j \langle g|$ at site j describes the coupling between $|g\rangle$ and $|r\rangle$ with Rabi frequency Ω, , $n_j \coloneqq |r\rangle_j \langle r|$ is a projector onto the Rydberg state at site j, and V_{jk} denotes the repulsive van der Waals interaction between Rydberg states at sites j and k that scales as $\sim R_{jk}^{-6}$ with the distance R_{jk} of two atoms. In this experiment, they observed peculiar behaviors of the particular initial state $|\mathbb{Z}_2\rangle \coloneqq |rgrg\cdots\rangle$. They observed that oscillations of states between $|\mathbb{Z}_2\rangle$ and the complementary state $|\mathbb{Z}_2'\rangle \coloneqq |grgr\cdots\rangle$ persist for a long time. They also measured the time evolution of the domain-wall density[1] and observed robust oscillations of it. In addition, they compared these results with the ones computed from a thermal ensemble. More

[1] Here, they defined the domain wall as two neighbouring atoms in the *same* state, which is different from its usual definition in, e.g., the ferromagnetic Ising model.

specifically, they estimated effective temperature from the experiment and computed the expectation values of observables in the canonical ensemble at the corresponding temperature. They found significant differences between the experimentally measured results and the ones computed in the canonical ensemble, from which they deduced that the $|\mathbb{Z}_2\rangle$ state is not thermal.

Such non-thermal behavior of QMBS is distinct from the ETH violations discussed in Chapter 1 in the following sense. First, the system has no local conserved quantities except the total energy, which implies the system is surely non-integrable. Second, the system is homogeneous and disorder-free, which rules out the possibility of MBL. Third, H_{Ryd} is "connected" when regarded as an adjacent matrix in the way explained in Sec. 1.3.3, and thus the Hilbert space is not fragmented. Conversely, we can define QMBS as their complement, and here we adopt the following definition:

> A QMBS model is one that exhibits non-thermal behavior, or more precisely, that has highly excited but ETH-violating eigenstates[2], even though it is not integrable, many-body localized, or fragmented (disconnected).

2.1.2 PXP model

On the theoretical side, an effective model for this system has attracted much attention since the experiment. This model is referred to as the PXP model [78, 79] described by the Hamiltonian

$$H_{\mathrm{PXP}} \coloneqq \sum_j P_{j-1} X_j P_{j+1}, \tag{2.2}$$

where $X_j = |g\rangle_j \langle r| + |r\rangle_j \langle g|$, and $P_j \coloneqq 1 - n_j = |g\rangle_j \langle g|$ is a projector onto the ground state at site j, prohibiting simultaneous excitations of neighboring atoms $|\dots rr \dots\rangle$. Such constraint is called the Rydberg blockade [80]. The effective Hamiltonian H_{PXP} is obtained from H_{Ryd} under the assumption of $V_{j,j+1} \gg \Omega \gg V_{j,j+2}$, i.e., in the case where the van der Waals interactions are strong enough between neighboring atoms but are negligible between ones that are further apart. Note that the van der Waals interaction decays more rapidly than, e.g., the Coulomb interaction that scales as $\sim R^{-1}$ with the distance R. Thus, it is a relatively short-range interaction, and we can take only neighboring Rydberg blockade into account by tuning the parameters.

In a series of papers (Refs. [78, 79]), they captured several peculiar behaviors of $|\mathbb{Z}_2\rangle$; much slower EE growth than that of other states such as $|gggg\dots\rangle$, long oscillations of the expectation value of the local correlation function $\langle Z_j Z_{j+1}\rangle$ ($Z_j \coloneqq |r\rangle_j \langle r| - |g\rangle_j \langle g|$),

[2] It is known that EE of ground states and low-lying excited states of gapped Hamiltonians with local interactions can obey the area law in general [74–77]. We rule out such a peculiar situation at zero temperature by focusing on eigenstates in the middle of the energy spectrum.

anomalously low-entangled eigenstates in the middle of the energy spectrum, and persistent revivals of the fidelity $|\langle\mathbb{Z}_2(t)|\mathbb{Z}_2(0)\rangle|^2 \coloneqq \left|\langle\mathbb{Z}_2(0)|\,\mathrm{e}^{\mathrm{i}H_{\mathrm{PXP}}t}\,|\mathbb{Z}_2(0)\rangle\right|^2$. They also found that the level-spacing statistics agrees well with the Wigner-Dyson distribution, and thus concluded that such non-thermal behaviors do not stem from integrability.

In Ref. [81], Lin and Motrunich found the exact scar state in the PXP model that can be written as a matrix product state (MPS). Here, we impose PBC[3], assume that the number of sites L is even, and combine two neighboring sites into one block site. Due to the Rydberg blockade, only three states $|O\rangle \coloneqq |gg\rangle$, $|R\rangle \coloneqq |gr\rangle$, and $|L\rangle \coloneqq |rg\rangle$ are allowed at each block. Then, the Hamiltonian can be rewritten in terms of block states as

$$\begin{aligned} H_{\mathrm{PXP}} &= \sum_{j=1}^{L/2} \left[(|R\rangle\langle O| + |O\rangle\langle R|)_j \otimes (1 - |L\rangle\langle L|)_{j+1} + (1 - |R\rangle\langle R|)_j \otimes (|L\rangle\langle O| + |O\rangle\langle L|)_{j+1}\right] \\ &= \sum_{j=1}^{L/2} (|R\rangle\langle O| + |O\rangle\langle R| + |L\rangle\langle O| + |O\rangle\langle L|)_j \\ &\quad - \sum_{j=1}^{L/2} \left[(|OL\rangle + |RO\rangle)\langle RL| + |RL\rangle(\langle OL| + \langle RO|)\right]_{j,j+1}. \end{aligned} \tag{2.3}$$

Let us observe that the state[4]

$$|\psi_{\mathrm{S}}\rangle \coloneqq \mathrm{tr}\big(\mathsf{A}_1\mathsf{A}_2\cdots\mathsf{A}_{L/2}\big), \quad \mathsf{A}_j = \begin{pmatrix} \sqrt{2}\,|R\rangle & -|O\rangle \\ |O\rangle & -\sqrt{2}\,|L\rangle \end{pmatrix}_j \tag{2.4}$$

is an exact eigenstate of H_{PXP} with eigenvalue 0. One can see from

$$\mathsf{A}_j\mathsf{A}_{j+1} = \begin{pmatrix} 2\,|RR\rangle - |OO\rangle & -\sqrt{2}\,|RO\rangle + \sqrt{2}\,|OL\rangle \\ \sqrt{2}\,|OR\rangle - \sqrt{2}\,|LO\rangle & -|OO\rangle + 2\,|LL\rangle \end{pmatrix}_{j,j+1} \tag{2.5}$$

that the $|\psi_{\mathrm{S}}\rangle$ satisfies the Rydberg constraint between neighboring blocks, i.e., $|RL\rangle$ never appears. In addition, any local states on two consecutive blocks are orthogonal to $|OL\rangle +$

[3]The exact scar MPS for OBC can also be constructed with slight modifications at the boundaries [81].

[4]This representation is equivalent to

$$|\psi\rangle = \sum_{s_1=R,O,L} \cdots \sum_{s_{L/2}=R,O,L} \mathrm{tr}\left(A_1^{[s_1]}\cdots A_{L/2}^{[s_1]}\right)|s_1\ldots s_{L/2}\rangle$$

$$\text{where} \quad A_j^{[R]} = \begin{pmatrix} \sqrt{2} & 0 \\ 0 & 0 \end{pmatrix},\ A_j^{[O]} = \begin{pmatrix} 0 & -1 \\ 1 & 0 \end{pmatrix},\ A_j^{[L]} \begin{pmatrix} 0 & 0 \\ 0 & -\sqrt{2} \end{pmatrix},$$

which is commonly used as well.

$|RO\rangle$. Thus, the second term in Eq. (2.3) acts on $|\psi_{\mathrm{S}}\rangle$ as 0, which leads to

$$\begin{aligned} H_{\mathrm{PXP}}\,|\psi_{\mathrm{S}}\rangle &= \sum_{j=1}^{L/2}(|R\rangle\langle O| + |O\rangle\langle R| + |L\rangle\langle O| + |O\rangle\langle L|)_j \,\mathrm{tr}\big(\mathsf{A}_1\mathsf{A}_2\cdots\mathsf{A}_{L/2}\big) \\ &= \sum_{j=1}^{L/2}\mathrm{tr}\big(\mathsf{A}_1\cdots\mathsf{A}_{j-1}\mathsf{F}_j\mathsf{A}_{j+1}\cdots\mathsf{A}_{L/2}\big), \end{aligned}$$

where

$$\mathsf{F}_j \coloneqq \begin{pmatrix} \sqrt{2}\,|O\rangle & -|R\rangle - |L\rangle \\ |R\rangle + |L\rangle & -\sqrt{2}\,|O\rangle \end{pmatrix}_j . \tag{2.6}$$

It is important to note

$$\mathsf{F}_j = \frac{1}{\sqrt{2}}(\sigma^x\mathsf{A}_j - \mathsf{A}_j\sigma^x), \tag{2.7}$$

where the Pauli matrix σ^x acts on the auxiliary space. It immediately leads to $H_{\mathrm{PXP}}\,|\psi_{\mathrm{S}}\rangle = 0$ with the cyclic property of the trace. This state is a highly excited state, since H_{PXP} anticommutes with $\prod_j Z_j$, and therefore the energy spectrum is symmetric around zero energy. Nevertheless, $|\psi_{\mathrm{S}}\rangle$ is an MPS and thus has the area-law EE, so it indeed violates the ETH.

2.2 Other Exact QMBS Models

In the previous section, we saw that the PXP model has exact scar states. In this section, we review other important exact results on QMBS.

2.2.1 Shiraishi-Mori construction

In Refs. [32, 82], Shiraishi and Mori proposed a systematic construction of QMBS Hamiltonians before the Rydberg experiment and subsequent theoretical works on the PXP model. The recipe for the construction is quite simple. Given a target Hilbert subspace $\mathcal{H}_{\mathrm{S}}$ spanned by low-entangled states $\{|\psi_{\mathrm{S},k}\rangle\}_k$, find a set of operators $\{P_j\}$ that satisfy

$$\bigcap_j \mathrm{Ker}\,P_j = \mathcal{H}_{\mathrm{S}}. \tag{2.8}$$

Operators P_j can be taken as projectors onto the orthogonal complement $\mathcal{H}_{\mathrm{S}}^{\perp}$, but not necessarily[5]. Then, for arbitrary local Hermitian operators h_j, the scarred Hamiltonian

[5]The construction is sometimes called the "projector embedding" [69] according to their original papers. However, as we will see below, it can be straightforwardly generalized to other operators than projectors, so here we call it the "Shiraishi-Mori construction".

is constructed as the sum of $P_j^\dagger h_j P_j$. One can also add an additional Hermitian operator H' that satisfies $[H', P_j] = 0$ for any j, and the constructed scarred Hamiltonian is

$$H_{\mathrm{S}} \coloneqq \sum_j P_j^\dagger h_j P_j + H'. \tag{2.9}$$

It follows from

$$P_j(H_{\mathrm{S}} \left|\psi_{\mathrm{S},k}\right\rangle) = P_j H' \left|\psi_{\mathrm{S},k}\right\rangle = H' P_j \left|\psi_{\mathrm{S},k}\right\rangle = 0 \tag{2.10}$$

that $\mathcal{H}_{\mathrm{S}}$ is invariant under the action of H_{S}. Therefore, unless H' induces so strong coupling between $|\psi_{\mathrm{S},k}\rangle$ that $\mathcal{H}_{\mathrm{S}}$ gets thermal, eigenstates of H_{S} on $\mathcal{H}_{\mathrm{S}}$ also have low EE. Nevertheless, for general h_j, eigenstates in $\mathcal{H}_{\mathrm{S}}$ are embedded into the middle of the energy spectrum, and H_{S} is non-integrable. Therefore, H_{S} can be called a QMBS Hamiltonian.

Let us see a concrete example of the Shiraishi-Mori construction. We start with a frustration-free Hamiltonian called the Majumdar-Ghosh model [83, 84], which is an $S = 1/2$ spin chain model with the Hamiltonian

$$H_{\mathrm{MG}} \coloneqq \sum_{j=1}^{L} P_{j-1,j,j+1}^{S=3/2}. \tag{2.11}$$

Here, $P_{j-1,j,j+1}^{S=3/2}$ is a projector onto the subspace where the total spin of the three sites $j-1, j$, and $j+1$ is $3/2$, or more explicitly,

$$P_{j-1,j,j+1}^{S=3/2} \coloneqq \frac{2}{3}(\mathbf{S}_{j-1}\cdot\mathbf{S}_j + \mathbf{S}_j\cdot\mathbf{S}_{j+1} + \mathbf{S}_{j-1}\cdot\mathbf{S}_{j+1}) + \frac{1}{2}, \tag{2.12}$$

and we impose PBC, i.e., $\mathbf{S}_0 \coloneqq \mathbf{S}_L, \mathbf{S}_{L+1} \coloneqq \mathbf{S}_1$, and assume that the number of sites L is even. The Majumdar-Ghosh model has the two unique ground states

$$|\psi_{\mathrm{S},1}\rangle \coloneqq \bigotimes_{j=1}^{L/2} \frac{(|\uparrow\downarrow\rangle - |\downarrow\uparrow\rangle)_{2j-1,2j}}{\sqrt{2}}, \tag{2.13}$$

$$|\psi_{\mathrm{S},2}\rangle \coloneqq \bigotimes_{j=1}^{L/2} \frac{(|\uparrow\downarrow\rangle - |\downarrow\uparrow\rangle)_{2j,2j+1}}{\sqrt{2}}. \tag{2.14}$$

Note that these two states have area-law EE, since they can be written as MPSs with bond dimension 1 or 2:

$$|\psi_{\mathrm{S},1}\rangle = \begin{pmatrix} |\uparrow\rangle & |\downarrow\rangle \end{pmatrix}_1 \begin{pmatrix} |\downarrow\rangle \\ -|\uparrow\rangle \end{pmatrix}_2 \cdots \begin{pmatrix} |\uparrow\rangle & |\downarrow\rangle \end{pmatrix}_{L-1} \begin{pmatrix} |\downarrow\rangle \\ -|\uparrow\rangle \end{pmatrix}_L \tag{2.15}$$

$$|\psi_{\mathrm{S},2}\rangle = \mathrm{tr}\left(\begin{pmatrix} |\downarrow\rangle \\ -|\uparrow\rangle \end{pmatrix}_1 \begin{pmatrix} |\uparrow\rangle & |\downarrow\rangle \end{pmatrix}_2 \cdots \begin{pmatrix} |\downarrow\rangle \\ -|\uparrow\rangle \end{pmatrix}_{L-1} \begin{pmatrix} |\uparrow\rangle & |\downarrow\rangle \end{pmatrix}_L \right) \tag{2.16}$$

One can embed these states into the middle of the spectrum of H_{S} by setting h_j as, for example, the XYZ interaction between nearest and next-nearest neighboring spins:

$$h_j = \sum_{\alpha=x,y,z} \left[J_1^\alpha (S_{j-1}^\alpha S_j^\alpha + S_j^\alpha S_{j+1}^\alpha) + J_2^\alpha (S_{j-2}^\alpha S_j^\alpha + S_j^\alpha S_{j+2}^\alpha) \right]. \tag{2.17}$$

They numerically confirmed that all states except $|\psi_{\mathrm{S},k}\rangle$ are thermal, and thus the model is surely non-integrable.

2.2.2 Restricted spectrum-generating algebra

Several results on exact QMBS, including spin chain models [85–87] and η-pairing scars in the Hubbard-like model [88, 89], can be explained by the concept called the *spectrum-generating algebra* (SGA) [69, 90] or the *dynamical symmetry* [91] in the *restricted* subspace. Here, we focus on the Affleck-Kennedy-Lieb-Tasaki (AKLT) model [92–94], which is a celebrated $S = 1$ spin chain model, in particular, in the context of the symmetry protected topological phases [95–98]. Even though the model is non-integrable, one can write down the exact unique ground state as an MPS. Recently, other exact highly excited but low-entangled eigenstates were found [99–101]. Thus, it turned out that the AKLT model is also a good example of exact QMBS models, although it would not be expected in the original context to support Haldane's conjecture [102, 103]. Here, we will see these scar states in a simpler way [104].

The Hamiltonian of the $S = 1$ AKLT model is defined as

$$H_{\mathrm{AKLT}} \coloneqq \sum_{j=1}^{L} P_{j,j+1}^{S=2}, \tag{2.18}$$

where $P_{j,j+1}^{S=2}$ is a projector onto the subspace where the total spin of neighboring spins at site j and $j+1$ is 2, and we impose PBC and assume that the number of sites L is even. The projector $P_{j,j+1}^{S=2}$ can be written in terms of spin operators as

$$\begin{aligned} P_{j,j+1}^{S=2} &= \frac{1}{24} (\mathbf{S}_j + \mathbf{S}_{j+1})^2 \left[(\mathbf{S}_j + \mathbf{S}_{j+1})^2 - 2 \right] \\ &= \frac{1}{3} + \frac{1}{2} \mathbf{S}_j \cdot \mathbf{S}_{j+1} + \frac{1}{6} (\mathbf{S}_j \cdot \mathbf{S}_{j+1})^2. \end{aligned} \tag{2.19}$$

It is known that the ground state $|G\rangle$ of the AKLT model is unique and can be written as an MPS:

$$|G\rangle \coloneqq \mathrm{tr}(\mathsf{A}_1 \cdots \mathsf{A}_L), \tag{2.20}$$

where

$$\mathsf{A}_j = \begin{pmatrix} |0\rangle & -\sqrt{2}\,|+\rangle \\ \sqrt{2}\,|-\rangle & -|0\rangle \end{pmatrix}_j, \tag{2.21}$$

and $|+\rangle, |0\rangle$, and $|-\rangle$ are eigenstates of S^z with eigenvalues $+1, 0$, and -1, respectively. Let us denote the two-site state at sites j and $j+1$ with the total spin S^{tot} and the total S^z component m^{tot} as $|S^{\mathrm{tot}}, m^{\mathrm{tot}}\rangle\rangle_{j,j+1}$, which can be written in terms of the S^z basis as follows:

$$
\begin{aligned}
&|2,2\rangle\rangle = |{+}{+}\rangle \\
&|2,1\rangle\rangle = \frac{1}{\sqrt{2}}(|{+}0\rangle + |0{+}\rangle) \qquad |1,1\rangle\rangle = \frac{1}{\sqrt{2}}(|{+}0\rangle - |0{+}\rangle) \\
&|2,0\rangle\rangle = \frac{1}{\sqrt{6}}(|{+}{-}\rangle + 2\,|00\rangle + |{-}{+}\rangle) \qquad |1,0\rangle\rangle = \frac{1}{\sqrt{2}}(|{+}{-}\rangle - |{-}{+}\rangle) \quad |0,0\rangle\rangle = \frac{1}{\sqrt{3}}(|{+}{-}\rangle - |00\rangle + |{-}{+}\rangle) \\
&|2,-1\rangle\rangle = \frac{1}{\sqrt{2}}(|0{-}\rangle + |{-}0\rangle) \qquad |1,-1\rangle\rangle = \frac{1}{\sqrt{2}}(|0{-}\rangle - |{-}0\rangle) \\
&|2,-2\rangle\rangle = |{-}{-}\rangle\,.
\end{aligned}
$$

One can easily see $H_{\mathrm{AKLT}}\,|G\rangle = 0$ from

$$
\mathsf{A}_j\mathsf{A}_{j+1} = \begin{pmatrix} |00\rangle - 2\,|{+}{-}\rangle & -\sqrt{2}\,|0{+}\rangle + \sqrt{2}\,|{+}0\rangle \\ \sqrt{2}\,|{-}0\rangle - \sqrt{2}\,|0{-}\rangle & -2\,|{-}{+}\rangle + |00\rangle \end{pmatrix}_{j,j+1} \tag{2.22}
$$

$$
= \begin{pmatrix} -\sqrt{2}|1,0\rangle\rangle - \sqrt{3}|0,0\rangle\rangle & 2|1,1\rangle\rangle \\ -2|1,-1\rangle\rangle & \sqrt{2}|1,0\rangle\rangle - \sqrt{3}|0,0\rangle\rangle \end{pmatrix}_{j,j+1}. \tag{2.23}
$$

Since $P^{S=2}_{j,j+1}$ is positive semi-definite, so is H_{AKLT}, and thus one can verify that $|G\rangle$ is indeed a ground state, although its uniqueness is nontrivial.

In fact, $(Q^+)^k\,|G\rangle$ ($k = 1, 2, \ldots, L/2$) are exact excited states with eigenvalues $2k$, where

$$
Q^+ \coloneqq \sum_{j=1}^{L} (-1)^j (S^+_j)^2. \tag{2.24}
$$

To see this, it suffices to show that

$$
\exp\bigl(-\alpha Q^+\bigr) H \exp\bigl(\alpha Q^+\bigr)\,|G\rangle = 2\alpha Q^+\,|G\rangle \tag{2.25}
$$

holds for arbitrary $\alpha \in \mathbb{C}$. It is because comparing the coefficients of α^n in both sides of

$$
H \exp\bigl(\alpha Q^+\bigr)\,|G\rangle = 2\alpha Q^+ \exp\bigl(\alpha Q^+\bigr)\,|G\rangle\,,
$$

one can obtain

$$
H(Q^+)^k\,|G\rangle = 2k(Q^+)^k\,|G\rangle\,. \tag{2.26}
$$

To prove Eq. (2.25), it is important to note that the series expansion of the exponential operator is finite:

$$
\begin{aligned}
\exp\bigl(\alpha Q^+\bigr) &= \prod_{j=1}^{L} \exp\Bigl[(-1)^j \alpha (S^+_j)^2\Bigr] \\
&= \prod_{j=1}^{L} \Bigl[1 + (-1)^j \alpha (S^+_j)^2\Bigr].
\end{aligned} \tag{2.27}
$$

Then, it can be verified straightforwardly that

$$\exp\left(-\alpha Q^{+}\right) P_{j,j+1}^{S=2} \exp\left(\alpha Q^{+}\right)|G\rangle = \mathrm{tr}(\mathsf{A}_1 \cdots \mathsf{A}_{j-1} \mathsf{M}_{j,j+1} \mathsf{A}_{j+2} \cdots \mathsf{A}_L), \tag{2.28}$$

where

$$\begin{aligned} \mathsf{M}_{j,j+1} &\coloneqq (-1)^j 4\alpha \begin{pmatrix} |2,2\rangle\rangle & 0 \\ |2,1\rangle\rangle & -|2,2\rangle\rangle \end{pmatrix} \\ &= (-1)^j \alpha [(S_j^+)^2 - (S_{j+1}^+)^2] \mathsf{A}_j \mathsf{A}_{j+1}. \end{aligned} \tag{2.29}$$

Therefore, one obtains

$$\begin{aligned} \exp\left(-\alpha Q^{+}\right) H \exp\left(\alpha Q^{+}\right)|G\rangle &= \sum_{j=1}^{L} \mathrm{tr}(\mathsf{A}_1 \cdots \mathsf{A}_{j-1} \mathsf{M}_{j,j+1} \mathsf{A}_{j+2} \cdots \mathsf{A}_L) \\ &= \left(\sum_{j=1}^{L} (-1)^j \alpha [(S_j^+)^2 - (S_{j+1}^+)^2] \right) \mathrm{tr}(\mathsf{A}_1 \cdots \mathsf{A}_L) \\ &= 2\alpha Q^{+}|G\rangle . \end{aligned}$$

In this way, Eq. (2.25) is proved.

Since $|G\rangle$ has area-law EE and Q^+ is just the sum of local operators, we expect that $(Q^+)^k|G\rangle$ also have low EE. In fact, it can be shown that EE of $(Q^+)^k|G\rangle$ is bounded by $\sim \ln(L)$ [100].

The above structure of scars is formalized as the *restricted spectrum generating algebra* (RSGA) [89, 90]. The Hamiltonian H_0 is said to have a SGA or a dynamical symmetry when it satisfies [105]

$$[H_0, Q^\dagger] = \omega Q^\dagger \tag{2.30}$$

with a certain operator $Q^\dagger$. The η operator [106–108] in the Fermi-Hubbard model is one of the examples:

$$[H_{\text{F-Hub}}, \eta^\dagger] = (U - 2\mu)\eta^\dagger, \tag{2.31}$$

where

$$H_{\text{F-Hub}} \coloneqq \sum_{\sigma=\uparrow,\downarrow} \left[-t \sum_{\langle \mathbf{r},\mathbf{r}' \rangle} (c_{\mathbf{r},\sigma}^\dagger c_{\mathbf{r}',\sigma} + \text{h.c.}) - \mu \sum_{\mathbf{r}} n_{\mathbf{r},\sigma} \right] + U \sum_{\mathbf{r}} n_{\mathbf{r},\uparrow} n_{\mathbf{r},\downarrow} \tag{2.32}$$

is a Fermi-Hubbard Hamiltonian on a d-dimensional cubic lattice, $\mathbf{r}$ stands for each site, $\langle \mathbf{r}, \mathbf{r}' \rangle$ denotes nearest-neighboring sites, $c_{\mathbf{r},\sigma}^\dagger$ and $c_{\mathbf{r},\sigma}$ are fermionic creation and annihilation operators at site $\mathbf{r}$, and

$$\eta^\dagger \coloneqq \sum_{\mathbf{r}} \mathrm{e}^{\mathrm{i}\boldsymbol{\pi}\cdot\mathbf{r}} c_{\mathbf{r},\uparrow}^\dagger c_{\mathbf{r},\downarrow}^\dagger, \tag{2.33}$$

with $\boldsymbol{\pi} = (\pi, \pi, \ldots, \pi)$. On the other hand, in the AKLT model, such an algebraic relation does not hold in the *entire* Hilbert space but in the *restricted* scarred subspace:

$$([H_{\mathrm{AKLT}}, Q^+] - 2Q^+)\mathcal{W} = 0, \tag{2.34}$$

where

$$\mathcal{W} = \mathrm{Span}\{(Q^+)^k \left|G\right\rangle \mid k = 0, 1, \ldots, L/2\}. \tag{2.35}$$

In general, the Hamiltonian H is said to exhibit a RSGA when it satisfies

$$([H, Q^\dagger] - \omega Q^\dagger)\mathcal{W} = 0, \tag{2.36}$$

with a certain operator $Q^\dagger$. Here, ω is an interval of scar states' energies, and $\mathcal{W} \subsetneq \mathcal{H}$ is a Hilbert subspace that is invariant under $Q^\dagger$, i.e., $Q^\dagger\mathcal{W} \subset \mathcal{W}$. Remind that the algebraic relation $[H, Q^\dagger] = \omega Q^\dagger$ does not necessarily hold in the full Hilbert space. In other words, $Q^\dagger$ is not associated with the entire symmetry of H but a rather "partial" symmetry which is valid only in the subspace $\mathcal{W}$. Then, given an energy eigenstate $\left|\psi_{\mathrm{S}}\right\rangle \in \mathcal{W}$ with eigenvalue E_0, one can obtain the tower of scar states $(Q^\dagger)^k \left|\psi_{\mathrm{S}}\right\rangle$ with eigenvalue $E_0 + k\omega$. If $\left|\psi_{\mathrm{S}}\right\rangle$ is low-entangled, then $(Q^\dagger)^k \left|\psi_{\mathrm{S}}\right\rangle$ is also expected to be low-entangled and thus athermal. However, the whole Hamiltonian does not have such a simple structure and can be decomposed as [69]

$$H = H_{\mathrm{scar}} \oplus H_{\mathrm{thermal}}, \tag{2.37}$$

where H_{scar} acts on $\mathcal{W}$ and H_{thermal} acts on $\mathcal{W}^\perp$.

2.3 Summary of the Chapter and Motivation of Our Work

We have reviewed QMBS with a brief historical context. In particular, we have looked through the pioneering experiment that directly observed QMBS features and its effective model called the PXP model. We have also reviewed the previous theoretical works on exact QMBS models, namely, the Shiraishi-Mori construction and the RSGA, providing their concrete examples.

Despite intensive studies including those discussed above, most of the exact QMBS models were limited to particular classes. For example, in most models, the dimension of the local Hilbert space is at most two or three. In addition, most models assume translational invariance. Therefore, it is a natural and important question to ask whether one can construct QMBS models under more general conditions, such as models with the higher local dimension or inhomogeneous ones.

Motivated by this question, in the following Chapters, we will propose a new family of QMBS models that are analytically tractable and also easy to generalize. The key to the

construction of our model is the so-called Onsager algebra, which originally appeared in obtaining the exact solution of the two-dimensional classical Ising model [109]. In Chapter 3, we will discuss the simplest case of our model, i.e., the $S = 1/2$ spin chain model with a one-parameter family of scar states. In Chapter 4, we will generalize it to higher S and multi-parameter scar states.

"Looking forward to things is half the pleasure of them."
– L. M. Montgomery, *Anne of Green Gables*

CHAPTER 3

QUANTUM MANY-BODY SCARRED MODEL WITH $S = 1/2$

In this Chapter, we propose a spin model with exact QMBS states. Our strategy for constructing a scarred model is as follows. We start with integrable spin chain models that themselves cannot be called QMBS models due to their integrability. Focusing on a certain operator, we can find appropriate perturbations that destroy the integrability but leave particular low-entangled states to be still eigenstates.

Our models have three remarkable features:

1. Scar states in our model are not product states but do have a finite sub-volume entanglement. In other words, our scars are not trivially ETH-violating states such as a vacuum state in the Fermi-Hubbard model.

2. Our models are easy to generalize to those with an arbitrary integer or half-integer spin quantum number S and multi-parameter scar states.

3. We do not impose translational invariance on our models. To the best of our knowledge, this is the first explicitly constructed example of such disordered QMBS models.

Although the Onsager algebra plays an important role to construct our model, the simplest $S = 1/2$ case can be understood without knowledge of it. Thus, we focus on the simplest case in this Chapter, and relegate the details of the Onsager algebra and the generalization of our models to Chapter 4.

3.1 Model

3.1.1 Unperturbed Hamiltonian and symmetry

We start with the $S = 1/2$ XX spin chain model described by the Hamiltonian [110, 111]

$$H_2 \coloneqq \sum_{j=1}^{L} \left(S_j^+ S_{j+1}^- + S_j^- S_{j+1}^+ \right). \tag{3.1}$$

Here, L is the number of sites and assumed to be even, and $S_j^\pm$ are raising/lowering operators acting on the local Hilbert space $\mathcal{H}_j \simeq \mathbb{C}^2$ at site j as

$$S_j^+ = \begin{pmatrix} 0 & 1 \\ 0 & 0 \end{pmatrix}_j, \quad S_j^- = \begin{pmatrix} 0 & 0 \\ 1 & 0 \end{pmatrix}_j. \tag{3.2}$$

We also impose PBC, i.e., $S_{L+1}^\pm \coloneqq S_1^\pm$. The subscript 2 of H denotes the dimension of the local Hilbert space at each site and is to be generalized to arbitrary $n \in \mathbb{N}$ in the next Chapter. It can be easily verified that H_2 commutes with the $\mathrm{U}(1)$-charge Q defined as

$$Q \coloneqq \sum_{j=1}^{L} S_j^z, \quad S_j^z = \begin{pmatrix} 1/2 & 0 \\ 0 & -1/2 \end{pmatrix}_j, \tag{3.3}$$

since $[Q, S_j^\pm] = \pm S_j^\pm$. In addition to Q, one can find another operator Q^+ defined as

$$Q^+ \coloneqq \sum_{j=1}^{L} (-1)^{j+1} S_j^+ S_{j+1}^+, \tag{3.4}$$

which also commutes with H_2. From $[H_2, Q^+] = 0$ and the fact that the ferromagnetic state $|\Downarrow\rangle \coloneqq \bigotimes_{j=1}^{L} |\downarrow\rangle$ is an eigenstate of H_2 with eigenvalue 0, one can see that $(Q^+)^k |\Downarrow\rangle$ ($k = 1, \ldots, L/2$) are also eigenstates of H_2 with eigenvalue 0 [1].

3.1.2 Perturbation and scarring

The XX chain itself is integrable, and thus it cannot be called a QMBS model. Let us try to find appropriate perturbations that destroy the integrability of H_2 but leave $(Q^+)^k |\Downarrow\rangle$ to be still eigenstates. The Hamiltonian of our QMBS model can be written as

$$H_{\mathrm{S},2} \coloneqq H_2 + H_{\mathrm{pert}} + h \sum_{j=1}^{L} S_j^z, \tag{3.5}$$

where the last term describing an external field is added to break the degeneracy among $(Q^+)^k |\Downarrow\rangle$.

[1] $Q^+ |\Downarrow\rangle$ is known as a singular state in the context of the Bethe ansatz for the Heisenberg chain [112–115].

To find such perturbations, it is important to note that $(Q^+)^k \left|\Downarrow\right\rangle$ have no overlap with

$$\left|\downarrow\uparrow\downarrow\right\rangle \quad \text{and} \quad \frac{\left|\downarrow\uparrow\uparrow\right\rangle + \left|\uparrow\uparrow\downarrow\right\rangle}{\sqrt{2}} \tag{3.6}$$

over three consecutive sites. It is because Q^+ raises adjacent spins and creates a bi-magnon with momentum $k = \pi$, and thus the above two states cannot appear in $(Q^+)^k \left|\Downarrow\right\rangle$. This fact can also be verified in an elegant way. Let us consider an (unnormalized) *coherent state*

$$\left|\psi(\beta)\right\rangle \coloneqq \exp\left(\beta^2 Q^+\right) \left|\Downarrow\right\rangle, \tag{3.7}$$

which of course belongs to $\operatorname{Span}\left\{\left|\Downarrow\right\rangle, Q^+ \left|\Downarrow\right\rangle, \ldots, (Q^+)^{L/2} \left|\Downarrow\right\rangle\right\}$. It is important to note that terms $S_j^+ S_{j+1}^+$ in Q^+ commute each other and that the series expansion of the exponential operator is finite. Then one can obtain the matrix product operator (MPO) representation of $\exp\left(\beta^2 Q^+\right)$ as follows:

$$\begin{aligned}
\exp\left(\beta^2 Q^+\right) &= \prod_{j=1}^{L} \exp\left[(-1)^{j+1} \beta^2 S_j^+ S_{j+1}^+\right] \\
&= \prod_{j=1}^{L} \left[1 + (-1)^{j+1} \beta^2 S_j^+ S_{j+1}^+\right] \\
&= \begin{pmatrix} 1 & \beta S_1^+ \end{pmatrix} \begin{pmatrix} 1 \\ \beta S_2^+ \end{pmatrix} \begin{pmatrix} 1 & -\beta S_2^+ \end{pmatrix} \begin{pmatrix} 1 \\ \beta S_3^+ \end{pmatrix} \cdots \begin{pmatrix} 1 & -\beta S_L^+ \end{pmatrix} \begin{pmatrix} 1 \\ \beta S_1^+ \end{pmatrix} \\
&= \operatorname{tr}(\mathsf{C}_1 \mathsf{C}_2 \cdots \mathsf{C}_L),
\end{aligned} \tag{3.8}$$

where

$$\mathsf{C}_j = \begin{pmatrix} 1 & (-1)^{j+1} \beta S_j^+ \\ \beta S_j^+ & 0 \end{pmatrix} \tag{3.9}$$

is a 2×2 matrix with entries in $\operatorname{End} \mathcal{H}_j$. Therefore, the coherent state is exactly written as an MPS:

$$\left|\psi(\beta)\right\rangle = \operatorname{tr}(\mathsf{A}_1 \mathsf{A}_2 \cdots \mathsf{A}_L), \tag{3.10}$$

where

$$\mathsf{A}_j = \begin{pmatrix} \left|\downarrow\right\rangle & (-1)^{j+1} \beta \left|\uparrow\right\rangle \\ \beta \left|\uparrow\right\rangle & 0 \end{pmatrix}_j \tag{3.11}$$

is a 2×2 matrix with entries in $\mathcal{H}_j$ (see also Fig. 3.1.) This MPS representation reveals that particular spin configurations over three consecutive sites never appear in $\left|\psi(\beta)\right\rangle$. To be specific, it is easily verified that

$$\mathsf{A}_{2j-1}\mathsf{A}_{2j}\mathsf{A}_{2j+1} = \begin{pmatrix} \left|\downarrow\downarrow\downarrow\right\rangle - \beta^2(\left|\downarrow\uparrow\uparrow\right\rangle - \left|\uparrow\uparrow\downarrow\right\rangle) & \beta \left|\downarrow\downarrow\uparrow\right\rangle + \beta^3 \left|\uparrow\uparrow\uparrow\right\rangle \\ \beta \left|\uparrow\downarrow\downarrow\right\rangle - \beta^3 \left|\uparrow\uparrow\uparrow\right\rangle & \beta^2 \left|\uparrow\downarrow\uparrow\right\rangle \end{pmatrix}_{2j-1,2j,2j+1}, \tag{3.12}$$

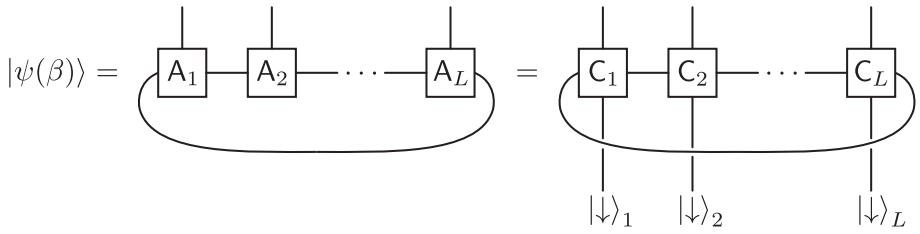

Figure 3.1: A graphical representation of an MPS for the coherent state.

and that any matrix elements of Eq. (3.12) are orthogonal to

$$|\downarrow\uparrow\downarrow\rangle \quad \text{and} \quad \frac{|\downarrow\uparrow\uparrow\rangle + |\uparrow\uparrow\downarrow\rangle}{\sqrt{2}}, \tag{3.13}$$

as we expected. The same conclusion follows from the spin configurations in $\mathsf{A}_{2j}\mathsf{A}_{2j+1}\mathsf{A}_{2j+2}$ as well. Therefore, we consider the following perturbation up to three-body interactions:

$$\begin{aligned} H_{\text{pert}} = \sum_{j=1}^{L} \Big\{ & c_j^{(1)} |\downarrow\uparrow\downarrow\rangle \langle\downarrow\uparrow\downarrow| \\ & + \frac{c_j^{(2)}}{2}(|\downarrow\uparrow\uparrow\rangle + |\uparrow\uparrow\downarrow\rangle)(\langle\downarrow\uparrow\uparrow| + \langle\uparrow\uparrow\downarrow|) \\ & + c_j^{(3)}[|\downarrow\uparrow\downarrow\rangle (\langle\downarrow\uparrow\uparrow| + \langle\uparrow\uparrow\downarrow|) + (|\downarrow\uparrow\uparrow\rangle + |\uparrow\uparrow\downarrow\rangle) \langle\downarrow\uparrow\downarrow|] \Big\}_{j-1,j,j+1}. \end{aligned} \tag{3.14}$$

Note that $H_{\text{S},2}$ does not have $\mathrm{U}(1)$ symmetry when $c_j^{(3)} \neq 0$. It is likely that the perturbation makes $H_{\text{S},2}$ non-integrable for generic $c_j^{(i)}$, which will be confirmed in the next section.

Several remarks are in order. First, we emphasize that the translational invariance is not assumed for $H_{\text{S},2}$. To the best of our knowledge, such models have not been explicitly constructed before this work[2]. Second, our model falls into the category of QMBS models induced by the RSGA discussed in Sec. 2.2.2. One can see that Eq. (2.36) holds for $H = H_{\text{S},2}, Q^\dagger = Q^+, \omega = 2h$, and $\mathcal{W} = \mathrm{Span}\{(Q^+)^k |\Downarrow\rangle \mid k = 0, \ldots, L/2\}$. Third, here we introduced a one-parameter coherent state, but it can be easily generalized to a multi-parameter one using higher Onsager-algebra elements to be discussed in the next Chapter. Fourth, our model can be mapped to a fermionic model via the Jordan-Wigner transformation. See Appendix A for its details.

[2]The exact scar states in the AKLT model with OBC were discussed in Refs. [99, 100]. However, it is almost translationally invariant, i.e., translationally invariant *in the bulk*.

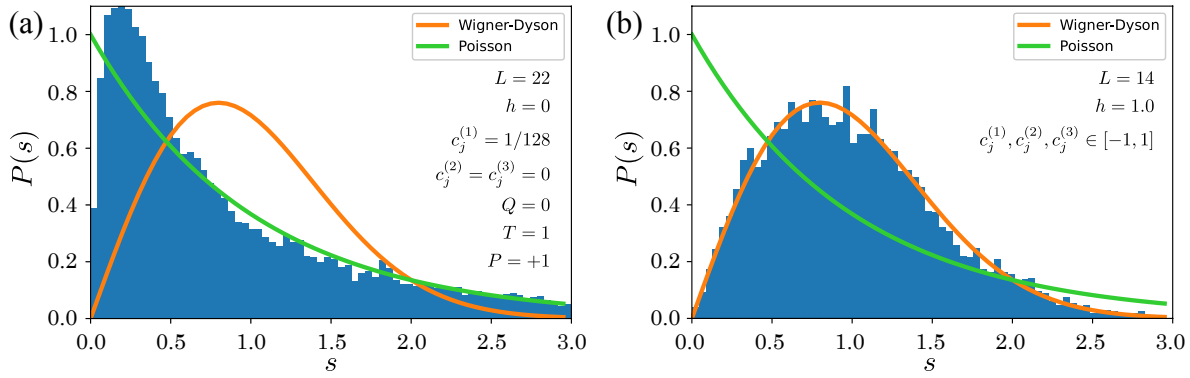

Figure 3.2: Comparison between level-spacing statistics of $H_{\mathrm{S},2}$ in (a) the nearly integrable case and those in (b) the generic case. (a) All the spectrum or (b) the middle half of the spectrum are used to obtain the statistics. In the left panel (a), very small perturbations $c_j^{(1)}$ are introduced to break the degeneracy. The parameters and the symmetry sector used are indicated in the figure, where T denotes the lattice translation and P denotes the spatial inversion. The probability density function of the Wigner-Dyson distribution $P_{\mathrm{WD}}(s) = (\pi/2)s\mathrm{e}^{-\pi s^2/4}$ and the Poisson distribution $P_{\mathrm{P}}(s) = \mathrm{e}^{-s}$ are shown for comparison. One can clearly see that the level-spacing statistics obey the Poisson distribution in (a) and the Wigner-Dyson distribution in (b).

3.2 Results

3.2.1 Level-spacing statistics

As mentioned in Chapter 2, we should distinguish QMBS models from integrable or MBL ones. To confirm that our model is neither integrable nor in the MBL phase, we compute the level-spacing statistics of $H_{\mathrm{S},2}$ by exact diagonalization in the particular case where $c_j^{(1)}, c_j^{(2)}$, and $c_j^{(3)}$ are chosen randomly from $[-1, 1]$. Here, we use the same notations for the level-spacing statistics as in Sec. 1.3.2, so let us briefly summarize these notations and well-known facts. Let $E_0 \leq E_1 \leq \cdots \leq E_j \leq \cdots$ be eigenenergies of $H_{\mathrm{S},2}$ in ascending order, $\Delta E_j \coloneqq E_{j+1} - E_j$ gaps between consecutive energy levels, and $\langle \Delta E \rangle$ the average of ΔE_j. The normalized energy level spacings $s_j \coloneqq \Delta E_j / \langle \Delta E \rangle$ are known to obey the Wigner Dyson distribution for non-integrable systems and the Poisson distribution for integrable or MBL systems [45, 51–55]. The r value $\langle r \rangle \coloneqq \langle \min(\Delta E_j, \Delta E_{j+1}) / \max(\Delta E_j, \Delta E_{j+1}) \rangle$ is used for quantitative detection of distribution statistics; $\langle r \rangle_{\mathrm{WD}} \simeq 0.536...$ for the Wigner-Dyson distribution, and $\langle r \rangle_{\mathrm{P}} \simeq 0.386...$ for the Poisson distribution [56, 57]. In Fig. 3.2, one can clearly see that the level-spacing statistics agree well with the Poisson distribution in the nearly integrable case (a), whereas the Wigner-Dyson distribution in the generic case (b). The r value of (b) $\langle r \rangle \simeq 0.5313...$ is also close enough to that of the Wigner-Dyson distribution. Therefore, we can deduce that our QMBS model is neither integrable nor in the MBL phase.

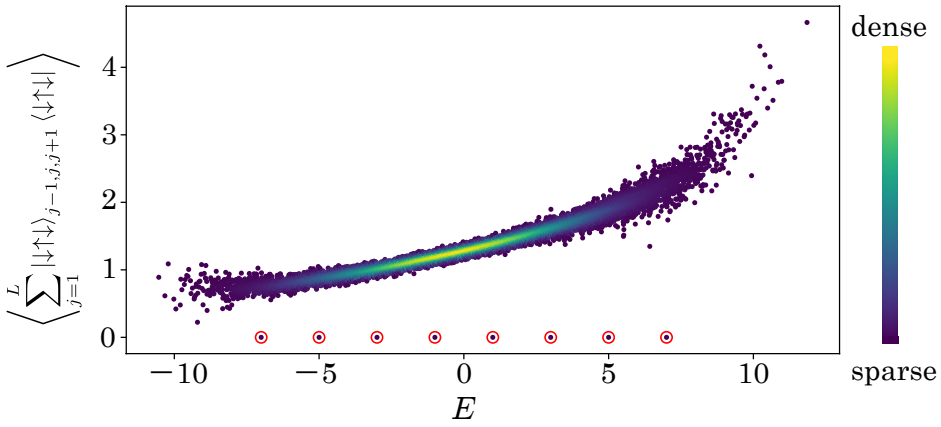

Figure 3.3: Expectation values of $\sum_{j=1}^{L} |\downarrow\uparrow\downarrow\rangle_{j-1,j,j+1} \langle\downarrow\uparrow\downarrow|$ for all energy eigenstates with energy E. Here, we set $L = 14$ and $h = 1.0$, and perturbation parameters $c_j^{(1)}$, $c_j^{(2)}$, and $c_j^{(3)}$ are randomly chosen from $[-1, 1]$. The color scale for each dot indicates the density of data points. The values for scar states $(Q^+)^k |\Downarrow\rangle$ $(k = 0, \dots 7)$ marked by red circles are exactly 0, and well separated from those for other typical states.

3.2.2 ETH violation in observables

The ETH implies that if two energy eigenstates are close in energy, then expectation values of any local observables for them should also be close. Here, let us see them in our model to illustrate athermal features. Figure 3.3 shows the expectation values of $\sum_{j=1}^{L} |\downarrow\uparrow\downarrow\rangle_{j-1,j,j+1} \langle\downarrow\uparrow\downarrow|$ for all energy eigenstates. One can see that expectation values for typical states form a curve with small fluctuation, while those for scar states $(Q^+)^k |\Downarrow\rangle$ $(k = 0, \dots 7)$ marked by red circles are exactly 0 and separated from them. This clearly demonstrates the ETH violation of our model.

3.2.3 Entanglement entropy

As discussed in Sec. 1.3.2, the von Neumann EE is one of the measures of quantum entanglement. Let us recall the definition and what we expect for its scaling. With respect to a bipartition of the system into subsystems A and $\bar{A}$, the von Neumann EE of $|\phi\rangle$ for A is defined as

$$\mathcal{S}_A := -\operatorname{tr}_A(\rho_A \ln \rho_A), \tag{3.15}$$

where $\rho_A := \operatorname{tr}_{\bar{A}}(|\phi\rangle \langle\phi|)$ is the reduced density matrix of region A. In the following, we focus on the half-chain bipartite von Neumann EE and take sites $j = 1, 2, \dots, L/2$ to be region A.

The strong ETH states that all energy eigenstates are thermal, which implies that these energy eigenstates have the volume-law entanglement [14] (see also Sec. 1.3.2).

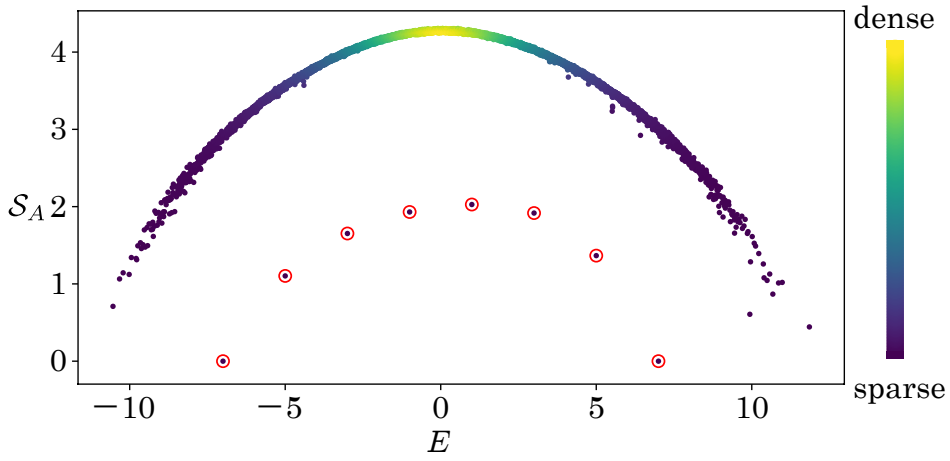

Figure 3.4: Half-chain bipartite EE as a function of energy E for $L = 14$ and $h = 1.0$. The color scale for each dot indicates the density of data points. $(Q^+)^k \left|\Downarrow\right\rangle$ $(k = 0, \ldots, L/2)$ are marked by red solid circles. Perturbation parameters are chosen randomly as $c_j^{(1)}, c_j^{(2)}, c_j^{(3)} \in [-1, 1]$.

Figure 3.4 shows half-chain bipartite EE for every energy eigenstate as a function of energy. One can clearly see a general feature of QMBS: most states in the bulk of the energy spectrum have large EE that is expected to obey a volume law, whereas atypical states $(Q^+)^k \left|\Downarrow\right\rangle$ have anomalously small EE marked by red circles [3]. We also investigate scalings of half-chain bipartite EE of thermal states and scar states with respect to the system size L, as shown in Fig. 3.5. Here, blue and orange dots indicate the highest EE of thermal states and that of scar states $(Q^+)^k \left|\Downarrow\right\rangle$ $(k = 0, \ldots, L/2)$ for given L, respectively. We can see that the EE of thermal states obeys a volume law, whereas that of scar states obeys a sub-volume law.

In Sec. 3.1.2, we derived the MPS representation of the coherent state $|\psi(\beta)\rangle$. Since the bond dimension, i.e., the dimension of the auxiliary space, of each matrix A_j is 2, $|\psi(\beta)\rangle$ has area-law EE. In the presence of an external field, however, not $|\psi(\beta)\rangle$ but $(Q^+)^k \left|\Downarrow\right\rangle$ is an eigenstate of $H_{\mathrm{S},2}$, so let us evaluate the EE of $(Q^+)^k \left|\Downarrow\right\rangle$. For simplicity, we assume that L is a multiple of 4 and impose the OBC for Q^+ only here. Although our model is valid only under the PBC, we expect that the boundary condition does not matter for the scaling of the EE. In addition, we apply to Q^+ the unitary transformation to obtain

$$U^\dagger Q^+ U = \sum_{j=1}^{L-1} S_j^+ S_{j+1}^+. \tag{3.16}$$

[3] The presence of excited eigenstates in integrable models that have area-law instead of volume-law entanglement has been pointed out early in Ref. [116].

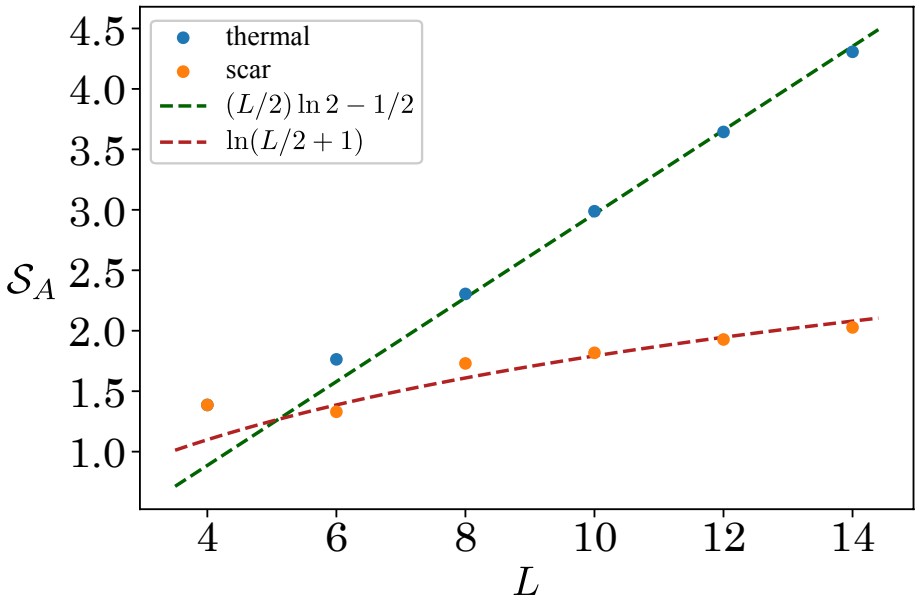

Figure 3.5: Finite-size scalings of half-chain bipartite EE with respect to the system size L. For given L, blue and orange dots indicate the highest EE of all energy eigenstates and that of scar states $(Q^+)^k \left|\Downarrow\right\rangle$ $(k = 0, \ldots, L/2)$, respectively. The green dashed line denotes the Page value $\mathcal{S}_{\text{Page}} = (L/2)\ln 2 - 1/2$ defined below in Eq. (3.34), and the red line is $\ln(L/2+1)$ in Eq. (3.31), the upper bound for EE of scar states under the OBC. One can clearly see that EE of thermal states represented by blue dots agree well with $\mathcal{S}_{\text{Page}}$, hence the volume-law scaling, whereas that of scar states scales as $\mathcal{O}(\ln L)$, i.e., the sub-volume-law scaling. Perturbation parameters are chosen randomly as $c_j^{(1)}, c_j^{(2)}, c_j^{(3)} \in [-1, 1]$.

Here, the unitary transformation

$$U \coloneqq \prod_{\substack{j=1 \\ j\equiv 1,2 \bmod 4}}^{L} \sigma_j^z = \sigma_1^z \otimes \sigma_2^z \otimes \mathbb{1}_3 \otimes \mathbb{1}_4 \otimes \cdots \otimes \sigma_{L-3}^z \otimes \sigma_{L-2}^z \otimes \mathbb{1}_{L-1} \otimes \mathbb{1}_L \tag{3.17}$$

is just a product of single-site rotations, and hence the EE of $(Q^+)^k \left|\Downarrow\right\rangle$ equals to that of $(U^\dagger Q^+ U)^k \left|\Downarrow\right\rangle$. It is important to note that $(U^\dagger Q^+ U)^k \left|\Downarrow\right\rangle$ can be written as the following MPS up to a constant factor:

$$(U^\dagger Q^+ U)^k \left|\Downarrow\right\rangle \propto \left|\xi(k)\right\rangle \coloneqq \sum_{s_1,\ldots,s_L=\uparrow,\downarrow} \langle\langle 0|M_1^{[s_1]} \cdots M_L^{[s_L]}|2k\rangle\rangle \left|s_1 \ldots s_L\right\rangle, \tag{3.18}$$

where

$$\left(M_j^{[\downarrow]}\right)_{\alpha\beta} = \begin{cases} \delta_{\alpha\beta} & \alpha\text{: even} \\ 0 & \alpha\text{: odd} \end{cases} = \frac{1+(-1)^\alpha}{2}\delta_{\alpha,\beta}, \quad \left(M_j^{[\uparrow]}\right)_{\alpha\beta} = \delta_{\alpha+1,\beta} \quad (\alpha, \beta = 0, 1, \ldots, 2k) \tag{3.19}$$

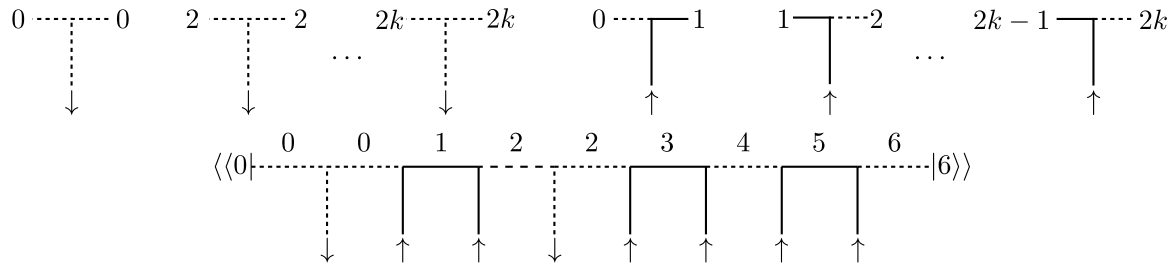

Figure 3.6: A graphical representation of $M_j^{[\updownarrow]}$ and an example of possible bond index configurations with $L = 8, k = 3$. Solid lines denote $|\uparrow\uparrow\rangle_{j,j+1} = S_j^+ S_{j+1}^+ |\downarrow\downarrow\rangle_{j,j+1}$ of adjacent two sites. One can see that the bond index runs from left to right as if it counts the number of up-spins.

is $(2k+1) \times (2k+1)$ matrices, and $\langle\langle 0|$ and $|2k\rangle\rangle$ denote the boundary indices of the auxiliary space. One has to be careful with *0-based indexing* here. Figure 3.6 may help you understand this representation. Since $M_j^{[\updownarrow]}$ does not depend on site j, we omit it in the following.

The numerical result suggests that the most entangled state of $(Q^+)^k |\Downarrow\rangle$ is $(Q^+)^{L/4} |\Downarrow\rangle$, i.e., a half-filling state. Thus, let us examine $|\xi(L/4)\rangle$ in detail. The Schmidt decomposition of $|\xi(L/4)\rangle$ is obtained by rewriting it as

$$|\xi(L/4)\rangle = \sum_{l=0}^{L/2} \left|\tilde{\phi}_{A,l}\right\rangle \otimes \left|\tilde{\phi}_{\bar{A},l}\right\rangle, \tag{3.20}$$

where

$$\left|\tilde{\phi}_{A,l}\right\rangle \coloneqq \sum_{s_1,\ldots,s_{L/2}} \langle\langle 0|M^{[s_1]} \cdots M^{[s_{L/2}]}|l\rangle\rangle \left|s_1 \ldots s_{L/2}\right\rangle, \tag{3.21}$$

$$\left|\tilde{\phi}_{\bar{A},l}\right\rangle \coloneqq \sum_{s_{L/2+1},\ldots,s_L} \langle\langle l|M^{[s_{L/2+1}]} \cdots M^{[s_L]}|L/2\rangle\rangle \left|s_{L/2+1} \ldots s_L\right\rangle. \tag{3.22}$$

To calculate the normalization factors of $\left|\tilde{\phi}_{A,l}\right\rangle$ and $\left|\tilde{\phi}_{\bar{A},l}\right\rangle$, let us define the transfer matrix

$$E_{(\alpha,\gamma)(\beta,\chi)} \coloneqq \sum_{s=\uparrow,\downarrow} \left(M^{[s]}\right)_{\alpha\beta} \left(M^{[s]}\right)^*_{\gamma\chi} = \frac{1+(-1)^\alpha}{2} \frac{1+(-1)^\gamma}{2} \delta_{\alpha\beta}\delta_{\gamma\chi} + \delta_{\alpha+1,\beta}\delta_{\gamma+1,\chi}. \tag{3.23}$$

Each normalization factor is

$$\left\langle\tilde{\phi}_{A,l}\middle|\tilde{\phi}_{A,l}\right\rangle = (E^{L/2})_{(0,0)(l,l)} \quad \text{and} \quad \left\langle\tilde{\phi}_{\bar{A},l}\middle|\tilde{\phi}_{\bar{A},l}\right\rangle = (E^{L/2})_{(l,l)(L/2,L/2)},$$

and in fact can be written as (see Appendix B)

$$(E^{L/2})_{(0,0)(l,l)} = c_l := \begin{cases} \binom{L/2 - l/2}{l/2} & l\text{: even} \\ \binom{L/2 - (l+1)/2}{(l-1)/2} & l\text{: odd} \end{cases}, \tag{3.24}$$

$$(E^{L/2})_{(l,l)(L/2,L/2)} = c_{L/2-l}. \tag{3.25}$$

Therefore, Eq. (3.20) reads

$$|\xi(L/4)\rangle = \sum_{l=0}^{L/2} \sqrt{c_l c_{L/2-l}}\, |\phi_{A,l}\rangle \otimes \left|\phi_{\bar{A},l}\right\rangle, \tag{3.26}$$

where

$$|\phi_{A,l}\rangle := \frac{\left|\tilde{\phi}_{A,l}\right\rangle}{\sqrt{\left\langle \tilde{\phi}_{A,l} \middle| \tilde{\phi}_{A,l} \right\rangle}} \quad \text{and} \quad \left|\phi_{\bar{A},l}\right\rangle := \frac{\left|\tilde{\phi}_{\bar{A},l}\right\rangle}{\sqrt{\left\langle \tilde{\phi}_{\bar{A},l} \middle| \tilde{\phi}_{\bar{A},l} \right\rangle}} \tag{3.27}$$

form an orthonormal set for region A and $\bar{A}$, respectively. Remarkably, the normalization factor of $|\xi(L/4)\rangle$ has a simple expression with the help of a generalized Vandermonde identity derived in Ref. [117]:

$$\langle \xi(L/4) | \xi(L/4) \rangle = \sum_{l=0}^{L/2} c_l c_{L/2-l} = \binom{(3/4)L}{L/4} =: \mathcal{N}. \tag{3.28}$$

Finally, we obtain a closed formula for the half-chain bipartite EE $\mathcal{S}_A$ of $(Q^+)^{L/4} |\Downarrow\rangle \propto |\xi(L/4)\rangle$:

$$\mathcal{S}_A = -\sum_{l=0}^{L/2} \frac{c_l c_{L/2-l}}{\mathcal{N}} \ln \frac{c_l c_{L/2-l}}{\mathcal{N}}. \tag{3.29}$$

Next, let us see how $\mathcal{S}_A$ scales with respect to L. One can obtain an upper bound of $\mathcal{S}_A$ by Gibbs' inequality [118]

$$-\sum_l p_l \ln p_l \le -\sum_l p_l \ln q_l, \tag{3.30}$$

which holds for any probability distributions $\{p_l\}$ and $\{q_l\}$ with equality if and only if $p_l = q_l$ for all l. By taking $p_l = c_l c_{L/2-l}/\mathcal{N}$ and $q_l = 1/(L/2+1)$, we obtain

$$\mathcal{S}_A \le -\sum_{l=0}^{L/2} \frac{c_l c_{L/2-l}}{\mathcal{N}} \ln\left(\frac{1}{L/2+1}\right) = \ln(L/2+1) = \mathcal{O}(\ln L). \tag{3.31}$$

Therefore, one can conclude that the EE of $(Q^+)^k |\Downarrow\rangle$ does not obey a volume law.

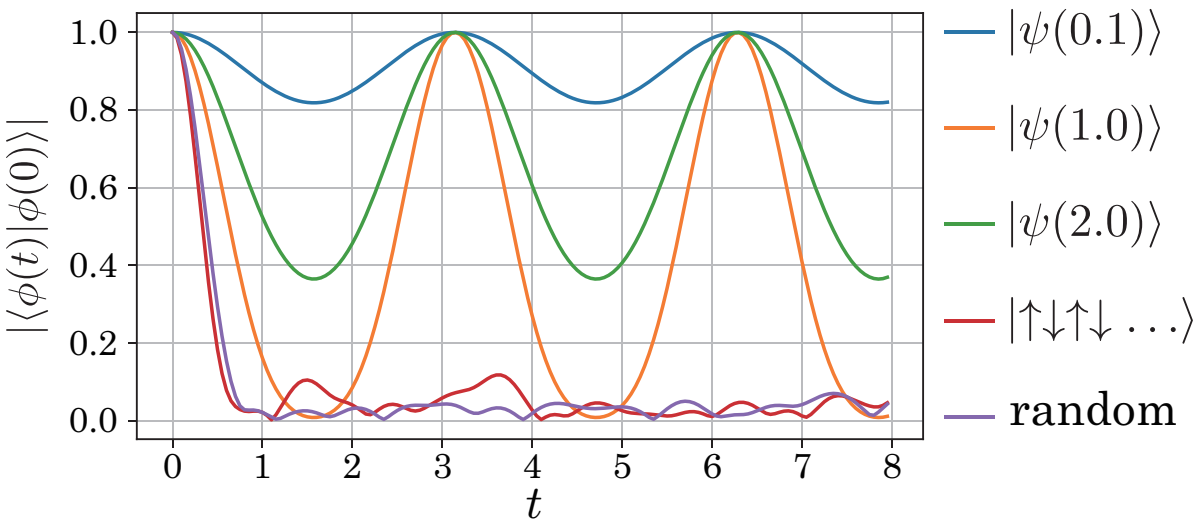

Figure 3.7: Fidelity dynamics with $L = 10,\ h = 1.0$, and $c_j^{(1)}, c_j^{(2)}, c_j^{(3)}$ chosen randomly from $[-1, 1]$. Perfectly periodic revivals can be seen in the case where the initial state is a coherent state, whereas for other typical states the fidelity decreases very quickly to 0.

3.2.4 Dynamics

The dynamics is also studied to illustrate the feature of the QMBS more explicitly. First, let us consider the dynamics of the coherent state. For the initial coherent state $|\psi_{t=0}(\beta)\rangle = |\psi(\beta)\rangle$, it is obvious from the construction of $H_{\mathrm{S},2}$ that

$$|\psi_t(\beta)\rangle = \mathrm{e}^{-\mathrm{i}H_{\mathrm{S},2}t}\,|\psi(\beta)\rangle = \mathrm{e}^{-\mathrm{i}hQt}\,|\psi(\beta)\rangle = \mathrm{e}^{\mathrm{i}hLt/2}\left|\psi(\mathrm{e}^{-\mathrm{i}ht}\beta)\right\rangle. \tag{3.32}$$

Although the coherent state does evolve, it returns to itself with period $T = \pi/h$, since $\left|\psi(\mathrm{e}^{\mathrm{i}\pi}\beta)\right\rangle = |\psi(\beta)\rangle$. We emphasize that this revival is perfect, and thus the coherent state never thermalizes.

We show in Fig. 3.7 the numerical results of the fidelity dynamics with several initial states $|\phi\rangle$ defined by

$$F(t) \coloneqq |\langle\phi(t)|\phi(0)\rangle| = \left|\langle\phi|\,\mathrm{e}^{\mathrm{i}H_{\mathrm{S},2}t}\,|\phi\rangle\right|. \tag{3.33}$$

When the initial states are coherent states, we can see perfectly periodic revivals of their fidelity. However, if the system starts from other generic states, its fidelity decreases rapidly to 0.

We also calculate the dynamics of the half-chain bipartite EE shown in Fig. 3.8 with the same setup as Fig. 3.7. It is easy to see that the coherent state does not gain entanglement, since $H_{\mathrm{S},2}$ acts on $|\psi(\beta)\rangle$ as if it is just an external field, i.e., a non-interacting term (see Eq. (3.32)). On the other hand, EE of the initial product state $|\uparrow\downarrow\uparrow\downarrow\ldots\rangle$ grows

soon and saturates near the Page value [119] of a random state

$$\mathcal{S}_{\text{Page}} = \frac{L}{2}\ln 2 - \frac{1}{2}. \tag{3.34}$$

From these numerical results on dynamics of the fidelity and EE, we confirm that typical states thermalize rapidly, whereas scar states never thermalize and violate ergodicity.

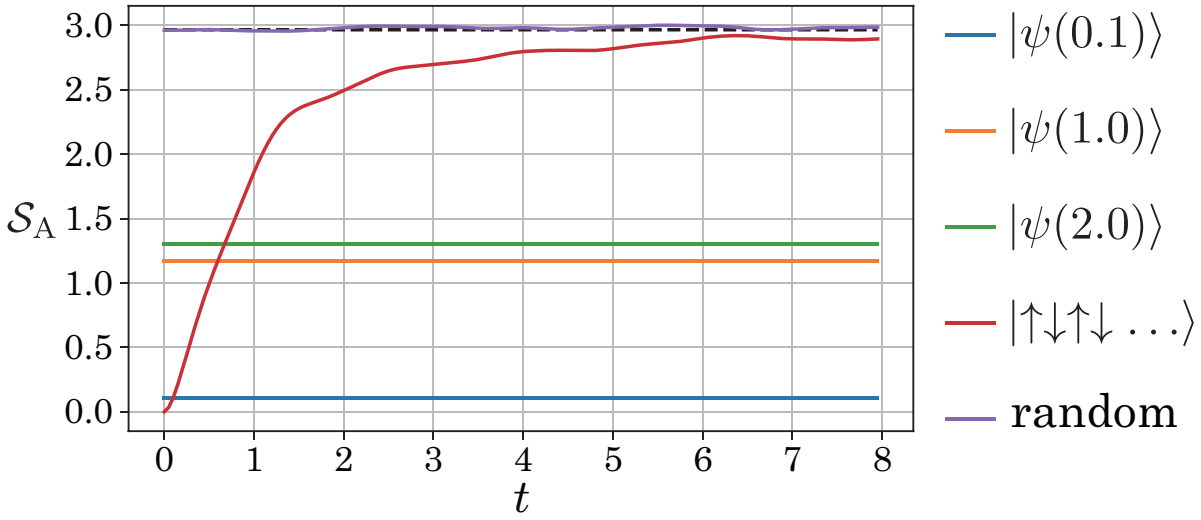

Figure 3.8: Dynamics of the half-chain bipartite EE with the same setup as Fig. 3.7. Initial coherent states have constant EE, while that of $|\uparrow\downarrow\uparrow\downarrow\ldots\rangle$ grows rapidly and saturates near the Page value denoted by the black dashed line. The EE of the random initial state almost remains at the Page value from the beginning to the end.

3.3 Summary of the Chapter

We have demonstrated the construction of our QMBS model in the simplest $S = 1/2$ case. We have begun with the integrable Hamiltonian H_2 and the operator Q^+ that commute with each other. We then have explicitly written down the coherent state associated with Q^+ as an MPS and found appropriate perturbation terms by observing local states at consecutive sites. We have illustrated various unusual behaviors in our model, providing both numerical and analytical results. The level-spacing statistics of the model obey the Wigner-Dyson distribution, and thus we have deduced that such peculiar behaviors are not due to integrability or MBL. Expectation values of an observable and EE have clearly distinguished scar states from other typical states. We have also investigated the dynamics of the fidelity and EE for several initial states. These results clearly illustrate the non-thermal behavior of scar states that are distinct from other thermal states. We emphasize that translational invariance is not needed in our model. To the best of our knowledge, this is the first explicitly constructed example of a disordered QMBS model.

Before closing our discussion, several remarks are in order. First, Onsager scar states $(Q^+)^k \left|\Downarrow\right\rangle$ can be prepared in a Markovian open quantum system. By taking jump operators that annihilate the coherent state, the decoherence-free subspace for this Lindblad dynamics is spanned by $(Q^+)^k \left|\Downarrow\right\rangle$. Thus, these Onsager scar states are steady states and can be obtained through this Markovian dynamics with arbitrary initial states. Second, for the $S = 1/2$ case, our coherent state and the ground state of the quantum lattice gas model studied in Ref. [120] are closely related to each other. In our coherent state, let us define bond variables for each bond between site j and $j+1$ by $b_{j,j+1} = (S_j^+ S_j^-)(S_{j+1}^+ S_{j+1}^-)$. Each $b_{j,j+1}$ takes 0 or 1, but one can easily see that adjacent bond variables $b_{j-1,j}$ and $b_{j,j+1}$ can never be 1 simultaneously. The configuration of $b_{j,j+1}$ corresponds to the ground state of the model in Ref. [120] by identifying $b_{j,j+1} = 1 \leftrightarrow \left|\uparrow\right\rangle_j$ and $b_{j,j+1} = 0 \leftrightarrow \left|\downarrow\right\rangle_j$. It is an open question whether we can apply similar identification to higher-spin cases discussed in the next Chapter.

"I often wonder why the whole world is so prone to generalise."
– Agatha Christie, *The Murder at the Vicarage*

CHAPTER 4

GENERALIZATION OF MODEL

In this Chapter, we generalize our model constructed in Chapter 3 to higher S models or multi-parameter scar states. Before going into the details, let us briefly summarize our strategy for constructing generalized QMBS models (see also Table 4.1.) The key is the so-called Onsager algebra, which originally appeared in obtaining the exact solution of a two-dimensional classical Ising model [109]. We start with spin chain models with the Onsager symmetry introduced recently [121]. Although they cannot be called QMBS models due to their integrability, by focusing on a certain Onsager-algebra element, we can add appropriate perturbations that destroy the integrability but leave particular low-entangled states to be still eigenstates. Our generalized QMBS models again turn out to be classified as those by the RSGA.

Table 4.1: Comparison between the original Hamiltonian H_n and the scarred Hamiltonian $H_{\mathrm{S},n}$.

	H_n	$\xrightarrow{+H_{\mathrm{pert}}}$	$H_{\mathrm{S},n}$
integrable	Yes		No
Onsager symmetry	Yes		Partially (RSGA)

In Sec. 4.1, we will briefly summarize the Onsager algebra and introduce unperturbed Hamiltonian with the Onsager symmetry. Next, we will see how to find appropriate perturbations in Sec. 4.2. Then, we will show several analytical and numerical results in Sec. 4.3.

4.1 Onsager Algebra and Clock Models with Onsager Symmetry

4.1.1 Onsager algebra

We first briefly introduce the Onsager algebra. The *two-dimensional classical* Ising model reduces to the *one-dimensional quantum* Ising model described by the following Hamiltonian

$$H_{\mathrm{QI}} = -h\sum_{j=1}^{L}\sigma_j^z - J\sum_{j=1}^{L}\sigma_j^x\sigma_{j+1}^x =: -hQ_{\mathrm{QI}} - J\hat{Q}_{\mathrm{QI}}, \tag{4.1}$$

which is called the quantum-classical correspondence [122]. Here, we impose the PBC, i.e., $\sigma_{L+1}^x \coloneqq \sigma_1^x$. One can find that the above Q_{QI} and $\hat{Q}_{\mathrm{QI}}$ satisfy the Dolan-Grady relation [123–125]

$$\begin{aligned}[\hat{Q}_{\mathrm{QI}},[\hat{Q}_{\mathrm{QI}},[\hat{Q}_{\mathrm{QI}},Q_{\mathrm{QI}}]]] &= 16[\hat{Q}_{\mathrm{QI}},Q_{\mathrm{QI}}],\\ [Q_{\mathrm{QI}},[Q_{\mathrm{QI}},[Q_{\mathrm{QI}},\hat{Q}_{\mathrm{QI}}]]] &= 16[Q_{\mathrm{QI}},\hat{Q}_{\mathrm{QI}}],\end{aligned} \tag{4.2}$$

which is known as a necessary and sufficient condition to generate the Onsager algebra. In Onsager's original notation, $A_0 \coloneqq Q_{\mathrm{QI}}$ and $A_1 \coloneqq \hat{Q}_{\mathrm{QI}}$ generate A_n and G_n which obey

$$\begin{aligned}[A_m,A_n] &= 4G_{m-n},\\ [A_m,G_n] &= 2A_{m-n} - 2A_{m+n},\\ [G_m,G_n] &= 0.\end{aligned} \tag{4.3}$$

4.1.2 Self-dual $\mathrm{U}(1)$-invariant clock model with Onsager symmetry

In Ref. [121], the authors found a series of clock models that respects the Onsager symmetry with the Hamiltonian

$$\begin{aligned}H_{\mathrm{orig},n} \coloneqq \mathrm{i}\sum_{j=1}^{L}\sum_{a=1}^{n-1}\frac{1}{1-\omega^{-a}}\Bigg[&(2a-n)\Big(\tau_j^a + (\sigma_j^\dagger\sigma_{j+1})^a\Big)\\ &+\sum_{b=1}^{n-1}\frac{1-\omega^{-ab}}{1-\omega^{-b}}\Big(\tau_j^a(\sigma_j^\dagger\sigma_{j+1})^b + (\sigma_j^\dagger\sigma_{j+1})^b\tau_{j+1}^a\Big)\Bigg]\end{aligned} \tag{4.4}$$

under the PBC, i.e., $\sigma_{L+1}=\sigma_1,\ \tau_{L+1}=\tau_1$. Here, $\omega \coloneqq \mathrm{e}^{2\pi\mathrm{i}/n}$ is one of the n-th roots of unity, L is the number of sites, and n is the dimension of each local Hilbert space $\mathcal{H}_j \simeq \mathbb{C}^n$, and hence the total Hilbert space is $\mathcal{H} = \bigotimes_{j=1}^{L}\mathcal{H}_j \simeq \mathbb{C}^{n^L}$. The operators σ_j and τ_j act on $\mathcal{H}_j$ as

$$\sigma = \begin{pmatrix} 0 & 1 & & \\ & \ddots & \ddots & \\ & & 0 & 1 \\ 1 & & & 0 \end{pmatrix}, \quad \tau = \begin{pmatrix} 1 & & & \\ & \omega & & \\ & & \ddots & \\ & & & \omega^{n-1} \end{pmatrix}, \tag{4.5}$$

and they satisfy

$$\sigma_j^n = \tau_j^n = 1, \tag{4.6}$$

$$\sigma_j^\dagger = \sigma_j^{n-1}, \quad \tau_j^\dagger = \tau_j^{n-1}, \tag{4.7}$$

$$\sigma_j\tau_j = \omega\tau_j\sigma_j, \quad \sigma_j\tau_k = \tau_k\sigma_j \ (j \neq k). \tag{4.8}$$

One can easily see from Eq. (4.4) that $H_{\mathrm{orig},n}$ is *self-dual*, i.e., invariant under the duality transformation

$$\tilde{\tau}_j = \sigma_j^\dagger\sigma_{j+1} \ (j = 1, \dots, L-1), \quad \tilde{\tau}_L = \sigma_L^\dagger, \quad \tilde{\sigma}_j = \prod_{k=1}^{L} \tau_k \tag{4.9}$$

up to boundary terms. In addition, $H_{\mathrm{orig},n}$ is $\mathrm{U}(1)$-*invariant*, i.e., commutes with the $\mathrm{U}(1)$ charge Q_{orig}:

$$Q_{\mathrm{orig}} \coloneqq \sum_{j=1}^{L} S_j^z = \sum_{j=1}^{L}\sum_{a=1}^{n-1} \frac{1}{1-\omega^{-a}} (\tau_j)^a, \tag{4.10}$$

where $S^z = \mathrm{diag}\left((n-1)/2, (n-3)/2, \dots, -(n-1)/2\right)$. This symmetry becomes clear by rewriting $H_{\mathrm{orig},n}$ as

$$H_{\mathrm{orig},n} = \mathrm{i}\sum_{j=1}^{L}\sum_{a=1}^{n-1} \frac{1}{1-\omega^{-a}} \left[(2a-n)\tau_j^a + n(S_j^+ S_{j+1}^-)^{n-a} - n(S_j^- S_{j+1}^+)^a\right]. \tag{4.11}$$

Here, we define

$$S_j^+ \coloneqq \sigma_j\left(1 - \frac{1}{n}\sum_{a=0}^{n-1}\tau_j^a\right) = \begin{pmatrix} 0 & 1 & & \\ & \ddots & \ddots & \\ & & 0 & 1 \\ 0 & & & 0 \end{pmatrix}_j, \quad S_j^- \coloneqq (S_j^+)^\dagger, \quad S_{L+1}^\pm \coloneqq S_1^\pm \tag{4.12}$$

which satisfy $[Q_{\mathrm{orig}}, S_j^\pm] = \pm S_j^\pm$, and hence $[Q_{\mathrm{orig}}, H_{\mathrm{orig},n}] = 0$. Note that $S^\pm$ are not standard spin raising/lowering operators and do not obey the $\mathrm{SU}(2)$ commutation relation, i.e., $[S^+, S^-] \not\propto S^z$ (except for the $n = 2$ or 3 case), and the model does not have $\mathrm{SU}(2)$ symmetry.

Due to the self-duality, $H_{\mathrm{orig},n}$ also commutes with $\hat{Q}_{\mathrm{orig}}$, the dual of Q_{orig} defined as

$$\hat{Q}_{\mathrm{orig}} \coloneqq \sum_{j=1}^{L}\sum_{a=1}^{n-1} \frac{1}{1-\omega^{-a}} (\sigma_j^\dagger\sigma_{j+1})^a. \tag{4.13}$$

Note that $[\hat{Q}_{\mathrm{orig}}, H_{\mathrm{orig},n}] = 0$ holds exactly even though the duality transformation has some subtleties at boundaries. Remarkably, Q_{orig} and $\hat{Q}_{\mathrm{orig}}$ satisfy the Dolan-Grady relation

$$\begin{aligned} [\hat{Q}_{\mathrm{orig}}, [\hat{Q}_{\mathrm{orig}}, [\hat{Q}_{\mathrm{orig}}, Q_{\mathrm{orig}}]]] &= n^2[\hat{Q}_{\mathrm{orig}}, Q_{\mathrm{orig}}], \\ [Q_{\mathrm{orig}}, [Q_{\mathrm{orig}}, [Q_{\mathrm{orig}}, \hat{Q}_{\mathrm{orig}}]]] &= n^2[Q_{\mathrm{orig}}, \hat{Q}_{\mathrm{orig}}]. \end{aligned} \tag{4.14}$$

Therefore, Q_{orig} and $\hat{Q}_{\mathrm{orig}}$ generate the Onsager algebra, and every Onsager-algebra element commutes with $H_{\mathrm{orig},n}$. To see this, it is illuminating to decompose $\hat{Q}_{\mathrm{orig}}$ into the sum of three terms as

$$\hat{Q}_{\mathrm{orig}} = Q^0_{\mathrm{orig}} + Q^+_{\mathrm{orig}} + Q^-_{\mathrm{orig}}, \tag{4.15}$$

where each term is defined as

$$Q^0_{\mathrm{orig}} \coloneqq \sum_{j=1}^{L}\sum_{a=1}^{n-1} \frac{1}{1-\omega^{-a}}\Big[(S^-_j S^+_{j+1})^a - \omega^{-a}(S^+_j S^-_{j+1})^a\Big], \tag{4.16}$$

$$Q^+_{\mathrm{orig}} \coloneqq \sum_{j=1}^{L}\sum_{a=1}^{n-1} \frac{1}{1-\omega^{a}}(S^+_j)^a (S^+_{j+1})^{n-a}, \quad Q^-_{\mathrm{orig}} \coloneqq (Q^+_{\mathrm{orig}})^\dagger. \tag{4.17}$$

One can easily verify

$$[Q_{\mathrm{orig}}, Q^0_{\mathrm{orig}}] = 0, \quad [Q_{\mathrm{orig}}, Q^\pm_{\mathrm{orig}}] = \pm n Q^\pm_{\mathrm{orig}}, \tag{4.18}$$

and this immediately leads to

$$\begin{aligned}
[Q_{\mathrm{orig}}, \hat{Q}_{\mathrm{orig}}] &= n(Q^+_{\mathrm{orig}} - Q^-_{\mathrm{orig}}),\\
[Q_{\mathrm{orig}}, [Q_{\mathrm{orig}}, \hat{Q}_{\mathrm{orig}}]] &= n^2(Q^+_{\mathrm{orig}} + Q^-_{\mathrm{orig}}),\\
[Q_{\mathrm{orig}}, [Q_{\mathrm{orig}}, [Q_{\mathrm{orig}}, \hat{Q}_{\mathrm{orig}}]]] &= n^3(Q^+_{\mathrm{orig}} - Q^-_{\mathrm{orig}}).
\end{aligned}$$

Therefore,

$$[Q_{\mathrm{orig}}, [Q_{\mathrm{orig}}, [Q_{\mathrm{orig}}, \hat{Q}_{\mathrm{orig}}]]] = n^2 [Q_{\mathrm{orig}}, \hat{Q}_{\mathrm{orig}}],$$

and then self-duality requires

$$[\hat{Q}_{\mathrm{orig}}, [\hat{Q}_{\mathrm{orig}}, [\hat{Q}_{\mathrm{orig}}, Q_{\mathrm{orig}}]]] = n^2 [\hat{Q}_{\mathrm{orig}}, Q_{\mathrm{orig}}].$$

In this way, the Dolan-Grady relation Eq. (4.14) holds.

4.1.3 Unitary transformation of $H_{\mathrm{orig},n}$

Although $H_{\mathrm{orig},n}$ is not symmetric under spatial inversion, one can obtain the inversion symmetric Hamiltonian up to boundaries by the unitary transformation:

$$\tilde{H}_n \coloneqq U^\dagger H_{\mathrm{orig},n} U \tag{4.19}$$

$$= -\sum_{j=1}^{L}\sum_{a=1}^{n-1} \frac{1}{2\sin(\pi a/n)}\Big\{ n(-1)^a\Big[(\tilde{S}^+_j \tilde{S}^-_{j+1})^a + (\tilde{S}^-_j \tilde{S}^+_{j+1})^a\Big] + (n-2a)\omega^{a/2}\tau^a_j\Big\}, \tag{4.20}$$

where

$$U \coloneqq \exp\left[\mathrm{i}\pi\left(1+\frac{1}{n}\right)\sum_{j=1}^{L} jS_j^z\right], \tag{4.21}$$

$$\tilde{S}_j^{\pm} \coloneqq S_j^{\pm}\ (j=1,\dots,L), \quad \tilde{S}_{L+1}^{\pm} \coloneqq (-1)^L \omega^{\pm L/2} S_1^{\pm}. \tag{4.22}$$

Although the boundary condition in $\tilde{H}_n$ is twisted, let us define untwisted Hamiltonian H_n under the PBC:

$$H_n \coloneqq -\sum_{j=1}^{L}\sum_{a=1}^{n-1}\frac{1}{2\sin(\pi a/n)}\left\{n(-1)^a\left[(S_j^+S_{j+1}^-)^a+(S_j^-S_{j+1}^+)^a\right]+(n-2a)\omega^{a/2}\tau_j^a\right\}. \tag{4.23}$$

The simplest $n=2$ case reduces to the $S=1/2$ XX chain model discussed in Chapter 3, and the $n=3$ case is known as a particular case of the Fateev-Zamolodchikov model [126, 127]. One can verify that H_n commutes with transformed Q^r_{orig} $(r=0,\pm)$ defined as

$$Q^0 \coloneqq \sum_{j=1}^{L}\sum_{a=1}^{n-1}\frac{(-1)^a}{\sin(\pi a/n)}\left[(S_j^-S_{j+1}^+)^a-(S_j^+S_{j+1}^-)^a\right], \tag{4.24}$$

$$Q^{\pm} \coloneqq \sum_{j=1}^{L}\sum_{a=1}^{n-1}\frac{(-1)^{(n+1)j+a}}{\sin(\pi a/n)}(S_j^{\pm})^a(S_{j+1}^{\pm})^{n-a}, \tag{4.25}$$

when L is even or n is odd. Therefore, we henceforth assume that L is even.

We denote by $|p\rangle$ $(p=0,1,\dots,n-1)$ the eigenstate of S^z with eigenvalue $p-(n-1)/2$. The ferromagnetic state $|\Downarrow\rangle \coloneqq \otimes_{j=1}^{L}|0\rangle$ is the eigenstate of H_n with eigenvalue $L\sum_{a=1}^{n-1} a\cot(\pi a/n)$. Since $[Q^+,H_n]=0$, $(Q^+)^k|\Downarrow\rangle$ are also eigenstates[1] of H_n with the same eigenvalue.

4.2 Generalized Scarred Model

4.2.1 $n>2$ case

Let us now generalize our QMBS Hamiltonian written as

$$H_{\mathrm{S},n} \coloneqq H_n + H_{\mathrm{pert}} + h\sum_{j=1}^{L} S_j^z \tag{4.26}$$

to that of higher n in a parallel way to Chapter 3. First, let us define an (unnormalized) coherent state

$$|\psi(\beta)\rangle \coloneqq \exp\left(\beta^n Q^+\right)|\Downarrow\rangle\,. \tag{4.27}$$

[1] It seems not so trivial to determine $k_{\max}$ such that $(Q^+)^{k_{\max}}|\Downarrow\rangle \neq 0$ and $(Q^+)^k|\Downarrow\rangle = 0$ for $k>k_{\max}$. Due to $Q \le L(n-1)/2$, $Q|\Downarrow\rangle = -L(n-1)/2$, and $[Q,Q^+]=nQ^+$, one can see $k_{\max} \le \lfloor \frac{n-1}{n}L \rfloor$. However, we have confirmed that $k_{\max} = \lfloor \frac{n-1}{n}L \rfloor$ does not always hold.

Similarly to the $n = 2$ case, $\exp(\beta^n Q^+)$ can be written as an MPO:

$$\exp\left(\beta^n Q^+\right) = \mathrm{tr}(\mathsf{C}_1 \mathsf{C}_2 \cdots \mathsf{C}_L), \tag{4.28}$$

where, for $0 \leq k, l \leq n-1$ (0-based indexing),

$$(\mathsf{C}_j)_{kl} = \begin{cases} (\beta S_j^+)^k & (l = 0) \\ \dfrac{(-1)^{(n+1)j+(n-l)}}{\sin[\pi(n-l)/n]} (\beta S_j^+)^{n+k-l} & (l \neq 0) \end{cases}, \tag{4.29}$$

or more explicitly,

$$\mathsf{C}_j = \begin{pmatrix} 1 & \frac{(-1)^{(n+1)j+(n-1)}}{\sin[\pi(n-1)/n]} (\beta S_j^+)^{n-1} & \frac{(-1)^{(n+1)j+(n-2)}}{\sin[\pi(n-2)/n]} (\beta S_j^+)^{n-2} & \cdots & \frac{(-1)^{(n+1)j+1}}{\sin[\pi/n]} (\beta S_j^+) \\ \beta S_j^+ & 0 & \frac{(-1)^{(n+1)j+(n-2)}}{\sin[\pi(n-2)/n]} (\beta S_j^+)^{n-1} & \cdots & \frac{(-1)^{(n+1)j+1}}{\sin[\pi/n]} (\beta S_j^+)^2 \\ (\beta S_j^+)^2 & 0 & 0 & \cdots & \frac{(-1)^{(n+1)j+1}}{\sin[\pi/n]} (\beta S_j^+)^3 \\ \vdots & \vdots & \vdots & \ddots & \vdots \\ (\beta S_j^+)^{n-2} & 0 & 0 & \cdots & \frac{(-1)^{(n+1)j+1}}{\sin[\pi/n]} (\beta S_j^+)^{n-1} \\ (\beta S_j^+)^{n-1} & 0 & 0 & \cdots & 0 \end{pmatrix}. \tag{4.30}$$

Therefore, the coherent state can be written as an MPS:

$$|\psi(\beta)\rangle = \mathrm{tr}(\mathsf{A}_1 \mathsf{A}_2 \cdots \mathsf{A}_L), \tag{4.31}$$

where for $0 \leq k, l \leq n-1$,

$$(\mathsf{A}_j)_{kl} = \begin{cases} \beta^k |k\rangle & (l = 0) \\ \dfrac{(-1)^{(n+1)j+(n-l)} \beta^{n+k-l}}{\sin[\pi(n-l)/n]} |n+k-l\rangle & (k+1 \leq l \leq n-1) \\ 0 & (\text{otherwise}) \end{cases}, \tag{4.32}$$

or more explicitly,

$$\mathsf{A}_j = \begin{pmatrix} |0\rangle & \frac{(-1)^{(n+1)j+(n-1)} \beta^{n-1}}{\sin[\pi(n-1)/n]} |n-1\rangle & \frac{(-1)^{(n+1)j+(n-2)} \beta^{n-2}}{\sin[\pi(n-2)/n]} |n-2\rangle & \cdots & \frac{(-1)^{(n+1)j+1} \beta}{\sin[\pi/n]} |1\rangle \\ \beta |1\rangle & 0 & \frac{(-1)^{(n+1)j+(n-2)} \beta^{n-1}}{\sin[\pi(n-2)/n]} |n-1\rangle & \cdots & \frac{(-1)^{(n+1)j+1} \beta^2}{\sin[\pi/n]} |2\rangle \\ \beta^2 |2\rangle & 0 & 0 & \cdots & \frac{(-1)^{(n+1)j+1} \beta^3}{\sin[\pi/n]} |3\rangle \\ \vdots & \vdots & \vdots & \ddots & \vdots \\ \beta^{n-2} |n-2\rangle & 0 & 0 & \cdots & \frac{(-1)^{(n+1)j+1} \beta^{n-1}}{\sin[\pi/n]} |n-1\rangle \\ \beta^{n-1} |n-1\rangle & 0 & 0 & \cdots & 0 \end{pmatrix}. \tag{4.33}$$

One can then find appropriate perturbations by examining local states on consecutive sites. In the case of $n = 3$, for example, the following states have no overlap with the coherent state:

$$\begin{gathered}
|010\rangle\,,\ |020\rangle\,,\ |110\rangle\,,\ |110\rangle\,,\ |011\rangle\,,|111\rangle\,,\\
\frac{1}{2}(|012\rangle + |021\rangle + |120\rangle + |210\rangle),\ \frac{1}{\sqrt{2}}(|012\rangle - |120\rangle),\ \frac{1}{\sqrt{2}}(|021\rangle - |210\rangle),\\
\frac{1}{2}(|022\rangle - |112\rangle - |211\rangle + |220\rangle),\ \frac{1}{2}(|022\rangle + |112\rangle - |211\rangle - |220\rangle),\\
\frac{1}{2\sqrt{2}}(|022\rangle + |112\rangle + 2\,|121\rangle + |211\rangle + |220\rangle),\\
\frac{1}{\sqrt{3}}(|122\rangle + |212\rangle + |221\rangle).
\end{gathered} \tag{4.34}$$

By using these, we can construct a perturbation term H_{pert}, which breaks $\mathrm{U}(1)$ symmetry in general. For a general n, it is easily verified that $|0\,p\,0\rangle$ $(p = 1, \ldots, n-1)$ does not appear in $|\psi(\beta)\rangle$.

4.2.2 Multi-parameter coherent state

We can also generalize the coherent state to the multi-parameter one. Let us see this in the case of $n = 2$. One can find Onsager-algebra elements

$$Q_l^+ \coloneqq \sum_{j=1}^{L} (-1)^{j+1} S_j^+ \left(\prod_{k=j+1}^{j+l-1} S_k^z \right) S_{j+l}^+. \tag{4.35}$$

Q_1^+ corresponds to Q^+ in Chapter 3. Then, we can construct a multi-parameter coherent state with Q_l^+'s:

$$\begin{aligned}
|\psi(\beta_1, \ldots, \beta_m)\rangle &\coloneqq \exp\left(\sum_{l=1}^{m} \beta_l^2 Q_l^+ \right) |\Downarrow\rangle \\
&= \left[\prod_{l=1}^{m} \exp\left(\beta_l^2 Q_l^+\right) \right] |\Downarrow\rangle\,.
\end{aligned} \tag{4.36}$$

Here, the second line follows from $[Q_k^+, Q_l^+] = 0$. Note that this state does not have overlap with

$$\left| \underbrace{\downarrow \ldots \downarrow}_{m} \uparrow \underbrace{\downarrow \ldots \downarrow}_{m} \right\rangle \tag{4.37}$$

over $(2m + 1)$ consecutive sites. Thus, we can construct a QMBS Hamiltonian by adding a perturbation term $\sum_{j=1}^{L} c_j \,|\downarrow \ldots \downarrow\uparrow\downarrow \ldots \downarrow\rangle_{j-m,\ldots,j+m} \langle\downarrow \ldots \downarrow\uparrow\downarrow \ldots \downarrow|$. As a more exotic situation than that in the one-parameter case, we have $\mathcal{O}(L^m)$ scar states written as $\left(\prod_{l=1}^{m} (Q_l^+)^{k_l}\right) |\Downarrow\rangle$, where $k_l \in \mathbb{N}$.

4.3 Results

4.3.1 $n = 3$ case

Here, as a demonstration of generalization to higher n, we show several results in the $n = 3$, or $S = 1$, case. In this case, the unperturbed Hamiltonian H_3 and the Onsager-algebra element Q^+ are

$$H_3 = \sqrt{3}\sum_{j=1}^{L}\left[S_j^+S_{j+1}^- + S_j^-S_{j+1}^+ - (S_j^+S_{j+1}^-)^2 - (S_j^-S_{j+1}^+)^2 - (S_j^z)^2 + \frac{2}{3}\right], \tag{4.38}$$

$$Q^+ = \frac{2}{\sqrt{3}}\sum_{j=1}^{L} S_j^+(S_j^+ - S_{j+1}^+)S_{j+1}^+. \tag{4.39}$$

Let us check in a parallel way to Chapter 3 that our generalized model for $n = 3$ possesses the characteristic features of QMBS.

4.3.1.1 Level-spacing statistics

To verify the non-integrability, we compute the level-spacing statistics. Figure 4.1 shows the level-spacing statistics of $H_{\mathrm{S},3}$ with all possible perturbations consisting of states in Eq. (4.34). One can see that the result of our model agrees well with the Wigner-Dyson distribution. Therefore, we can conclude that $H_{\mathrm{S},3}$ is also non-integrable.

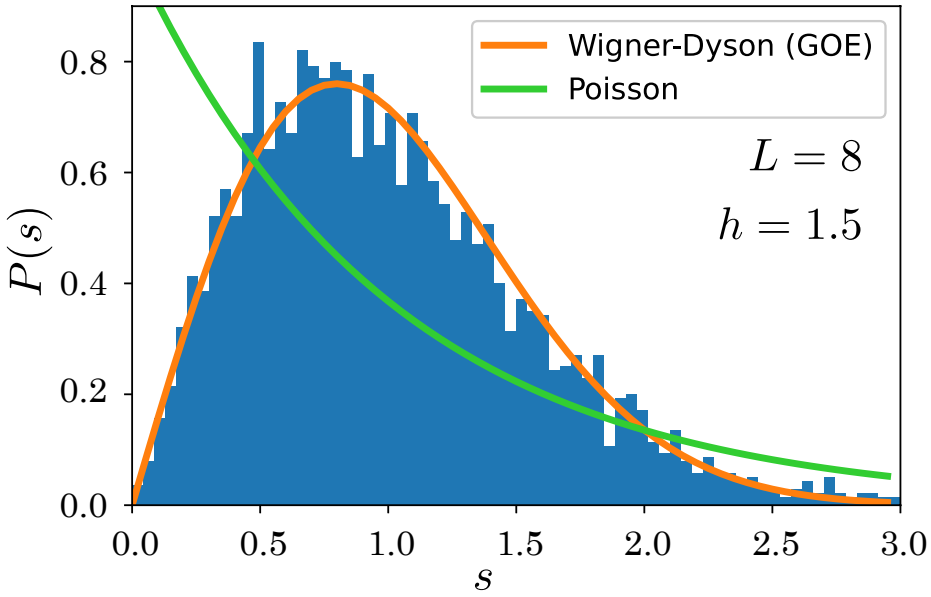

Figure 4.1: Level-spacing statistics in the middle half of the spectrum of $H_{\mathrm{S},3}$ with $L = 8$, and $h = 1.5$. All possible perturbations consisting of states in Eq. (4.34) are included. The result is in good agreement with the Wigner-Dyson distribution.

4.3.1.2 Entanglement entropy

Figure 4.2 shows half-chain bipartite EE for every energy eigenstate as a function of energy. In (a), one can see other low EE states besides $(Q^+)^k \left|\Downarrow\right\rangle$. In particular, EE of several states is exactly $\ln 2$. In fact, these are one-magnon states lying on the Hilbert subspace

$$\mathcal{H}_{\text{one-mag}} \coloneqq \text{Span}\{\left|1222\ldots22\right\rangle, \left|2122\ldots22\right\rangle, \left|2212\ldots22\right\rangle, \ldots, \left|2222\ldots21\right\rangle\}. \tag{4.40}$$

One can easily verify that if we do not use the last one of Eq. (4.34) for perturbation terms, then H_{pert} vanishes on $\mathcal{H}_{\text{one-mag}}$. These one-magnon scars, however, disappear when H_{pert} includes terms using the last one, as shown in (b).

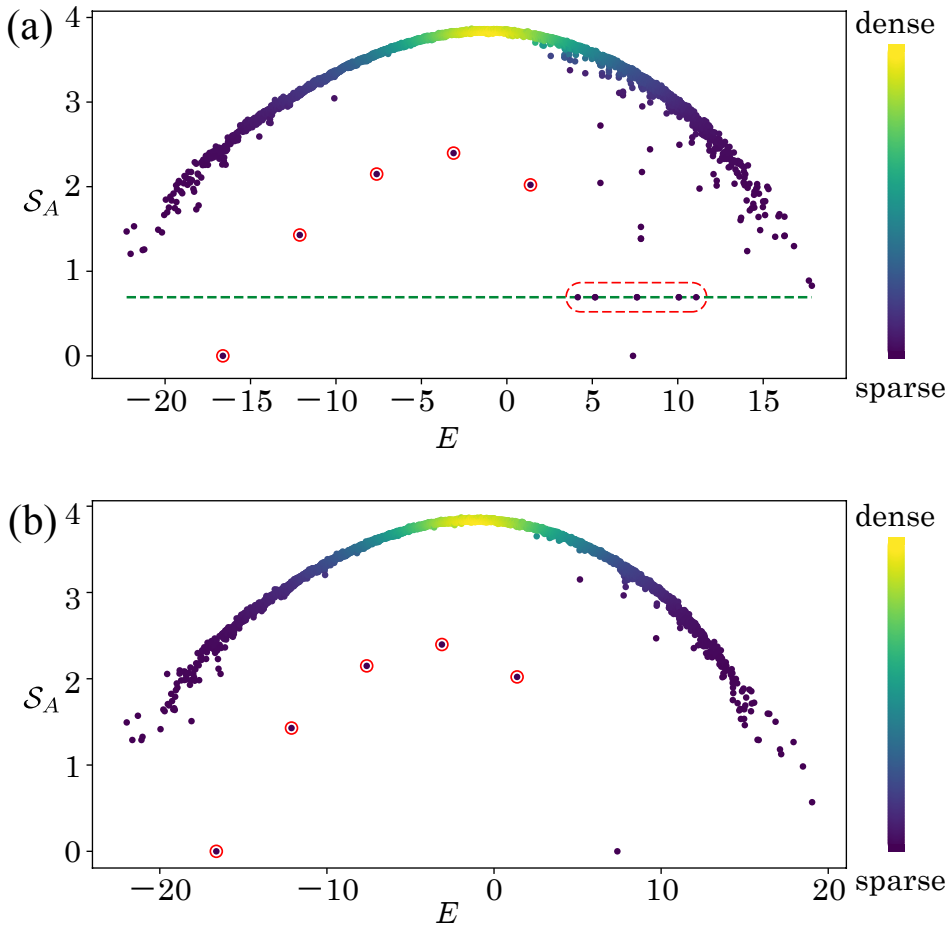

Figure 4.2: Half-chain bipartite EE as a function of energy E for $n = 3,\ L = 8,\ h = 1.5$. Color scale for each dot indicates the density of data points. $(Q^+)^k \left|\Downarrow\right\rangle$ are marked by red solid circles. In (a), perturbations are chosen not to destroy one-magnon scars indicated by the red dashed circle. A green dashed line indicates $\ln 2$. In (b), all possible perturbations are added, and then one-magnon states are no longer eigenstates.

4.3.1.3 Dynamics

Here, we show numerical results of the dynamics of the fidelity (Fig. 4.3) and EE (Fig. 4.4) in the case of $n = 3$. One can clearly see similar behaviors to the $n = 2$ case, that is, perfect revivals of the fidelity and unchanged EE for coherent states. Such behaviors of coherent states are distinct from those of other typical states, for which the fidelity rapidly decays to 0 and EE grows and saturates quickly to the Page value

$$\mathcal{S}_{\mathrm{Page}} = (L/2)\ln n - 1/2 \quad (\text{here } n = 3). \tag{4.41}$$

The perfect fidelity revivals of the coherent state follow from

$$|\psi_t(\beta)\rangle = \mathrm{e}^{-\mathrm{i}H_{\mathrm{St},n}}|\psi(\beta)\rangle \propto \mathrm{e}^{-\mathrm{i}hQt}|\psi(\beta)\rangle \propto \left|\psi(\mathrm{e}^{-\mathrm{i}ht}\beta)\right\rangle \tag{4.42}$$

and $\left|\psi(\omega^{-1}\beta)\right\rangle = |\psi(\beta)\rangle$, and hence the revival period $T = 2\pi/(nh)$, which is consistent with numerical results shown in Fig. 4.3. The steady EE is explained in the same way as the $n = 2$ case: all terms in $H_{\mathrm{S},n}$ act on $|\psi(\beta)\rangle$ as a constant except for $h\sum_{j=1}^{L} S_j^z$ and thus no entanglement is generated for $|\psi(\beta)\rangle$. These results are summarized as follows. The system typically forgets the initial state through the dynamics and eventually thermalizes. In contrast, coherent states consisting of scar states $(Q^+)^k|\Downarrow\rangle$ are trapped in a perfectly periodic orbit in the Hilbert subspace and never thermalize. These results clearly demonstrate the validity of the construction of our QMBS model even for the $n = 3$ case.

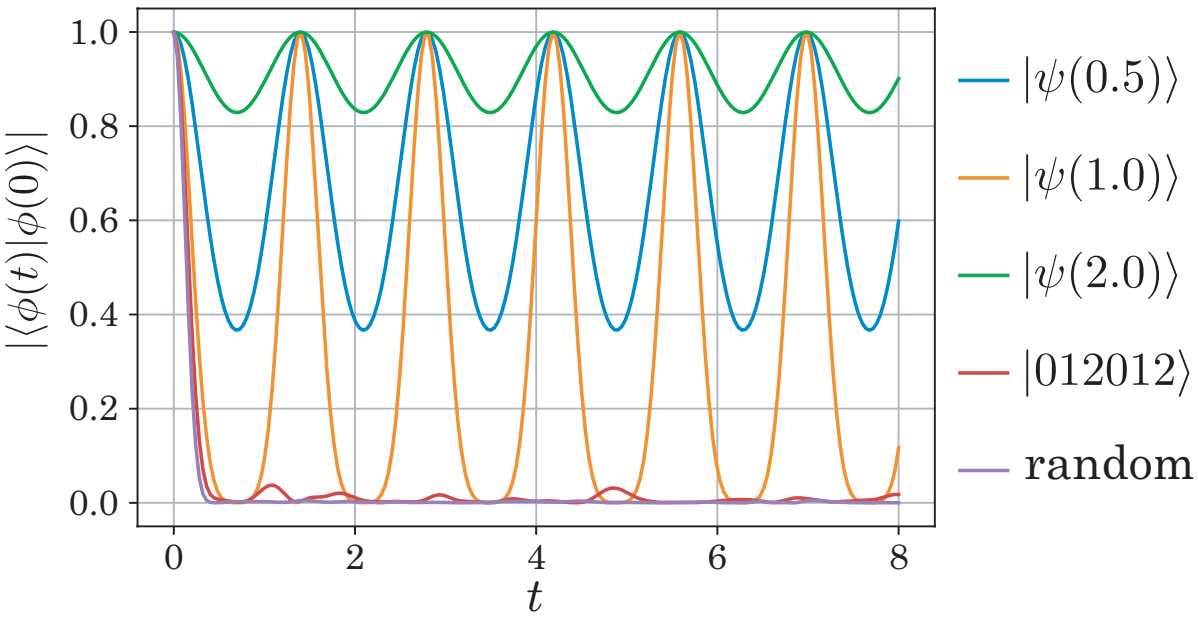

Figure 4.3: Fidelity dynamics with $n = 3,\ L = 6,\ h = 1.5$, and randomly chosen perturbation terms. The coherent states have perfect revivals with period $2\pi/(nh) \simeq 1.4$. On the other hand, for other typical states such as $|012012\rangle$ and a randomly chosen state, the fidelity decays to 0 rapidly.

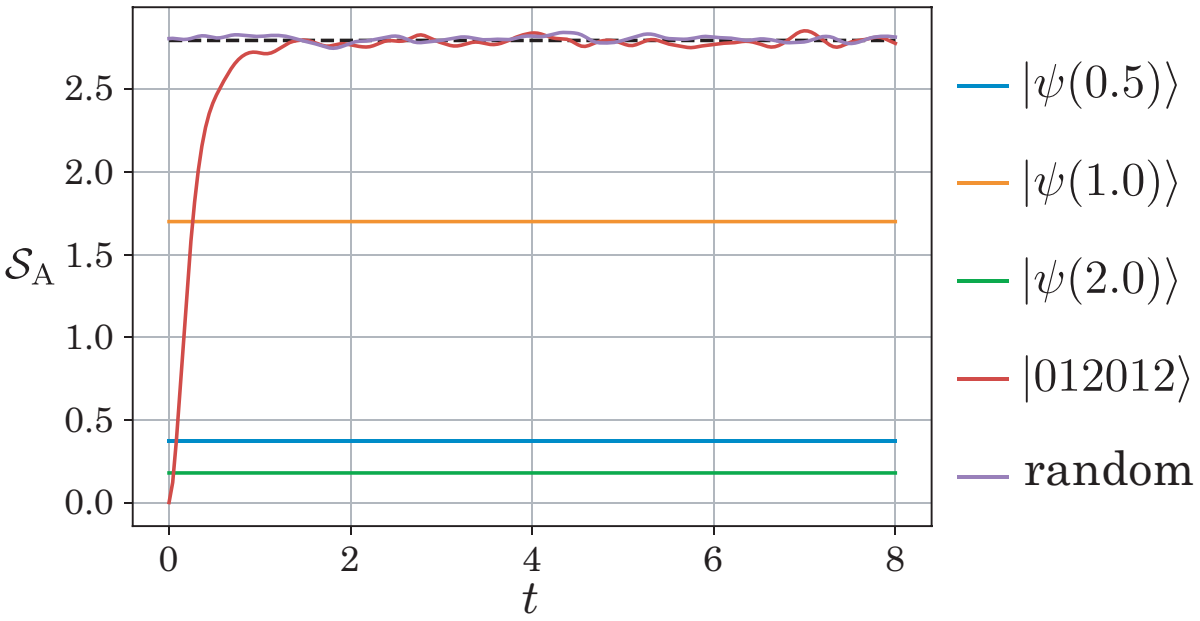

Figure 4.4: Dynamics of the half-chain bipartite EE with the same setup as Fig. 4.3. The Page value denoted by the black dashed line for $n = 3$ is $\mathcal{S}_\mathrm{Page} = (L/2)\ln 3 - 1/2$.

4.3.2 Multi-parameter coherent state

Next, we demonstrate the two-parameter coherent state with $S = 1/2$. Using Q_1^+ and Q_2^+, we can construct a two-parameter coherent state

$$|\psi(\beta_1, \beta_2)\rangle \coloneqq \exp\left(\beta_1^2 Q_1^+\right) \exp\left(\beta_2^2 Q_2^+\right) |\Downarrow\rangle \,. \tag{4.43}$$

Similarly to the one-parameter case, this two-parameter coherent state can be written as an MPS state, since $\exp\left(\beta_1^2 Q_1^+\right) \exp\left(\beta_2^2 Q_2^+\right)$ can be written as an MPO:

$$\exp\left(\beta_1^2 Q_1^+\right) \exp\left(\beta_2^2 Q_2^+\right) = \mathrm{tr}(\mathsf{D}_1 \dots \mathsf{D}_L), \tag{4.44}$$

where

$$\mathsf{D}_j = \begin{cases} \begin{pmatrix} 1 & \beta_1 S_j^+ \\ \beta_1 S_j^+ & 0 \end{pmatrix} \otimes \begin{pmatrix} 1 & \beta_2 S_j^+ \\ \beta_2 S_j^+ & 0 \end{pmatrix} \otimes \begin{pmatrix} 1 & 0 \\ 0 & -S_j^z \end{pmatrix} & (j : \text{odd}) \\ \begin{pmatrix} 1 & -\beta_1 S_j^+ \\ \beta_1 S_j^+ & 0 \end{pmatrix} \otimes \begin{pmatrix} 1 & 0 \\ 0 & S_j^z \end{pmatrix} \otimes \begin{pmatrix} 1 & \beta_2 S_j^+ \\ \beta_2 S_j^+ & 0 \end{pmatrix} & (j : \text{even}) \end{cases} \tag{4.45}$$

is an 8×8 matrix with entries in $\mathrm{End}\,\mathcal{H}_j$. The MPS representation of $|\psi(\beta_1, \beta_2)\rangle$ tells us that the coherent state has an overlap with neither

$$|00100\rangle \quad \text{nor} \quad \frac{|00101\rangle - |10100\rangle}{\sqrt{2}}. \tag{4.46}$$

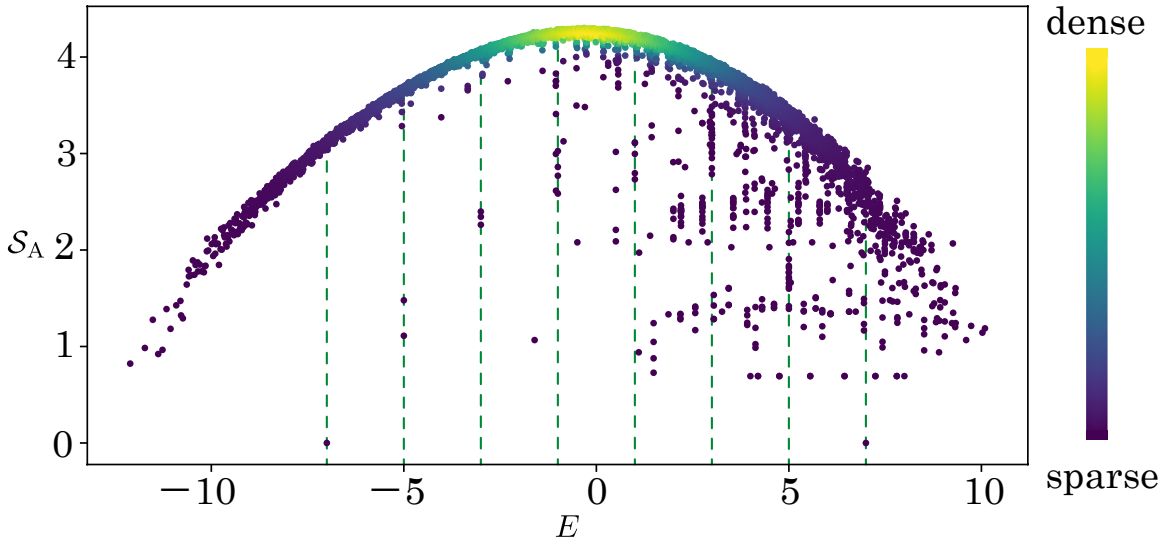

Figure 4.5: Half-chain bipartite EE for $n = 2$, $L = 14, h = 1.0$ with perturbations consisting of states in Eq. (4.46). Green dashed lines denote exact eigenvalues $-7, -5, \ldots, 7$ of scar states $(Q_1^+)^{k_1}(Q_2^+)^{k_2} |\Downarrow\rangle$. There seem to exist other scar states, but we have not identified them yet.

Then, adding the perturbation made from these states, we can construct a QMBS Hamiltonian in a similar way. Figure 4.5 shows the EE of this model. One can see much more anomalously low-entangled states than those in Fig. 3.4. Scar states $(Q_1^+)^{k_1}(Q_2^+)^{k_2} |\Downarrow\rangle$ are on the green dashed lines, but there seem to be other low-entangled states. It is an open question whether we can identify these other scar states in a simple way such as MPSs.

4.4 Summary of the Chapter

We have generalized the QMBS model constructed in Chapter 3 to higher S models and multi-parameter scar states, making full use of the Onsager algebra. First, we have introduced the Onsager symmetric Hamiltonian H_n with the dimension n of the local Hilbert space at each site. Focusing on certain Onsager-algebra elements, we have constructed generalized coherent states that can have multiple parameters. We have seen that these generalized coherent states can also be written as MPS, and then we have added appropriate perturbation terms to H_n to make the Hamiltonian non-integrable but particular low-entangled states still eigenstates. We then checked the validity of these generalized models in a parallel way to Chapter 3, such as the level-spacing statistics, EE, and dynamics. Through these results, we have found more exotic situations than the simplest case. In the $n = 3$ case, we have seen that additional one-magnon scar states can emerge with a particular perturbation. In the case where we considered higher Onsager-

algebra elements with multi-parameter coherent states, we found that much more scar states of the order of $\mathcal{O}(L^m)$ $(m \geq 2)$ can arise than if we take into account only one Onsager-algebra element, in which case the number of scar states is the order of $\mathcal{O}(L)$.

"The conclusion of things is the good. The good is, in other words, the conclusion at which all things arrive."
– Haruki Murakami, *1Q84*

CHAPTER 5

SUMMARY

In this Chapter, we summarize our results in the thesis and provide an outlook. We have constructed a new class of QMBS models without translational invariance. The key to the construction of our model was the Onsager algebra. Although it was originally used to solve exactly the two-dimensional classical Ising model, we have utilized it for constructing exact QMBS models. We have started with the Hamiltonian H_n, which respects the Onsager symmetry, and certain Onsager-algebra elements Q_l^+ that commute with H_n. While H_n is integrable, we added particular perturbations that break the integrability but keep a tower of several states generated by Q_l^+ still eigenstates of the perturbed Hamiltonian $H_{\mathrm{S},n}$.

In Chapter 3, we have studied the simplest $n = 2$ or $S = 1/2$ case in details. The level-spacing statistics clearly obey the Wigner-Dyson distribution, which implies that $H_{\mathrm{S},2}$ is indeed non-integrable. Nonetheless, scar states exhibit atypical behaviors, which were captured by eigenstate expectation values of an observable and half-chain bipartite EE. Moreover, the dynamics of the fidelity and EE were calculated for scar states and other typical states. Both results indicated that coherent states cannot escape from the scarred subspace and never thermalize, whereas other typical states rapidly get thermal.

In Chapter 4, we have investigated the generalized case, i.e., higher n models and multi-parameter coherent states. Similarly to Chapter 3, we have captured an athermal behavior from EE of eigenstates. In addition, we found intriguing situations that did not appear in the simplest case. For higher n, we have shown that additional scar states may emerge from the one-magnon subspace. For the multi-parameter generalization with higher Onsager-algebra elements, we have seen more scar states of the order of $\mathcal{O}(L^m)$ $(m \geq 2)$ than the one-parameter case where there are just $\mathcal{O}(L)$ scar states.

Our work suggests a number of future research directions. The unperturbed Hamil-

tonian has an infinite number of Onsager-algebra elements commuting with each other. This implies that one could extend our construction to various models. One of such examples is Floquet scars [128–130], which violate the Floquet version of ETH (Floquet-ETH). In addition, generalizations of the Onsager algebra have been discussed [131, 132], so one might be able to construct QMBS models using such generalized Onsager algebras. Another direction is an experimental implementation of Onsager's scars. In Ref. [133], the authors mention the link between scars appearing in a certain effective Rydberg model and Onsager's scars in the $n = 2$ case. Then, it will be interesting to consider experimental realizations of Onsager's scars for $n > 2$.

APPENDIX A

FERMIONIC ONSAGER'S SCARS

In Chapter 3, we have constructed the $S = 1/2$ spin model with QMBS states. Here, we derive a fermionic QMBS model via the Jordan-Wigner transformation. Spin operators can be rewritten in terms of fermionic creation/annihilation operators $a_j^\dagger$ and a_j as

$$S_j^+ = \exp\left(\mathrm{i}\pi \sum_{k=1}^{j-1} n_k\right) a_j^\dagger,\ S_j^- = \exp\left(\mathrm{i}\pi \sum_{k=1}^{j-1} n_k\right) a_j,\ S_j^z = n_j - \frac{1}{2}. \tag{A.1}$$

Here, $n_j \coloneqq a_j^\dagger a_j$ is the number operator at site j, and $a_j^\dagger$ and a_j satisfy $\{a_j, a_k^\dagger\} = \delta_{jk}$. Then, the unperturbed Hamiltonian H_2 is recast as

$$H_2 = \sum_{j=1}^{L-1} (a_j^\dagger a_{j+1} + a_{j+1}^\dagger a_j) - (-1)^F (a_L^\dagger a_1 + a_1^\dagger a_L), \tag{A.2}$$

where $F \coloneqq \sum_{j=1}^{L} n_j$ is the total number of fermions, and thus $(-1)^F$ represents the fermionic parity, which commutes with H_2. One can see that the boundary condition of H_2 for fermions is periodic in the odd-parity sector and anti-periodic in the even-parity sector.

The perturbation terms can also be rewritten in terms of fermions as

$$\sum_{j=1}^{L} c_j^{(1)} \left|\downarrow\uparrow\downarrow\right\rangle_{j-1,j,j+1} \left\langle\downarrow\uparrow\downarrow\right| = \sum_{j=1}^{L} c_j^{(1)} (1-n_{j-1}) n_j (1-n_{j+1}) \tag{A.3}$$

$$\begin{aligned}
&\sum_{j=1}^{L} \frac{c_j^{(2)}}{2} (\left|\downarrow\uparrow\uparrow\right\rangle + \left|\uparrow\uparrow\downarrow\right\rangle)_{j-1,j,j+1} (\left\langle\downarrow\uparrow\uparrow\right| + \left\langle\uparrow\uparrow\downarrow\right|) \\
&\qquad = \sum_{j=2}^{L-1} \frac{c_j^{(2)}}{2} \Big[(n_{j+1}-n_{j-1})^2 n_j - a_{j+1}^\dagger n_j a_{j-1} - a_{j-1}^\dagger n_j a_{j+1} \Big] \\
&\qquad\quad + \frac{c_1^{(2)}}{2} \Big[(n_2 - n_L)^2 n_1 - (-1)^F a_2^\dagger n_1 a_L - (-1)^F a_L^\dagger n_1 a_2 \Big] \\
&\qquad\quad + \frac{c_L^{(2)}}{2} \Big[(n_1 - n_{L-1})^2 n_L + (-1)^F a_1^\dagger n_L a_{L-1} + (-1)^F a_{L-1}^\dagger n_L a_1 \Big].
\end{aligned} \tag{A.4}$$

Thus, our QMBS Hamiltonian corresponds to a fermionic model with correlated hopping [134–136] up to boundary terms. The $U(1)$-breaking perturbation term

$$\sum_{j=1}^{L} c_j^{(1)} c_j^{(3)} [\left|\downarrow\uparrow\downarrow\right\rangle (\left\langle\downarrow\uparrow\uparrow\right| + \left\langle\uparrow\uparrow\downarrow\right|) + (\left|\downarrow\uparrow\uparrow\right\rangle + \left|\uparrow\uparrow\downarrow\right\rangle) \left\langle\downarrow\uparrow\downarrow\right|]_{j-1,j,j+1} \tag{A.5}$$

also breaks the parity $(-1)^F$ symmetry, and as a result, it contains non-local terms when it is mapped to fermionic operators.

We also consider untwisted fermionic QMBS model, since under PBC, i.e., $a_{L+1} = a_1$,

$$H_2' \coloneqq \sum_{j=1}^{L} (a_j^\dagger a_{j+1} + a_{j+1}^\dagger a_j) \tag{A.6}$$

$$Q'^{+} \coloneqq \sum_{j=1}^{L} (-1)^{j+1} a_j^\dagger a_{j+1}^\dagger \tag{A.7}$$

commute each other.

APPENDIX B

DERIVATION OF EQ. (3.24)

In this appendix, we derive Eq. (3.24)

$$(E^N)_{(0,0)(l,l)} = c_l := \begin{cases} \binom{N - l/2}{l/2} & l\text{: even} \\ \binom{N-(l+1)/2}{(l-1)/2} & l\text{: odd} \end{cases},$$

where

$$E_{(\alpha,\gamma)(\beta,\chi)} = \frac{1+(-1)^\alpha}{2}\frac{1+(-1)^\gamma}{2}\delta_{\alpha\beta}\delta_{\gamma\chi} + \delta_{\alpha+1,\beta}\delta_{\gamma+1,\chi} \quad (0 \le \alpha,\beta,\gamma,\chi \le N), \tag{B.1}$$

and we assume that $N = L/2$ is even and $0 \le l \le N$. The formula of $(E^N)_{(l,l)(N,N)}$ is also obtained in a similar way. The key to the derivation is that computing $(E^N)_{(0,0)(l,l)}$ is mapped to counting the number of lattice paths on the lattice shown in Fig. B.1. Each path is from $(0,0)$ to (N,l) with up-steps $(1,1)$ ($\nearrow$) and horizontal steps $(1,0)$ ($\rightarrow$), but no horizontal steps on odd y lines are allowed. One can see that the first term $[(1+(-1)^\alpha)/2][(1+(-1)^\gamma)/2]\delta_{\alpha\beta}\delta_{\gamma\chi}$ in Eq. (B.1) corresponds to $\rightarrow$, and the second term $\delta_{\alpha+1,\beta}\delta_{\gamma+1,\chi}$ to $\nearrow$. In the case of even l, each path reads a sequence that consists of $l\times\ \nearrow$ and $(N-l)\times\ \rightarrow$ under the restriction that the number of consecutive $\nearrow$'s should be even. Thus, by introducing $\nearrow\!\!\!\!\nearrow := \nearrow\nearrow$, the number of such lattice paths reduces to the number of combination of $l/2\times\ \nearrow\!\!\!\!\nearrow$ and $(N-l)\times\ \rightarrow$, resulting in c_l in the case of even l. When l is odd, the last step of every path should be $\nearrow$ because $\rightarrow$ are prohibited on odd y lines. Therefore, $(E^N)_{(0,0)(l,l)}$ equals the number of lattice paths from $(0,0)$ to $(N-1,l-1)$, i.e., the number of combination of $(l-1)/2\times\ \nearrow\!\!\!\!\nearrow$ and $(N-l)\times\ \rightarrow$.

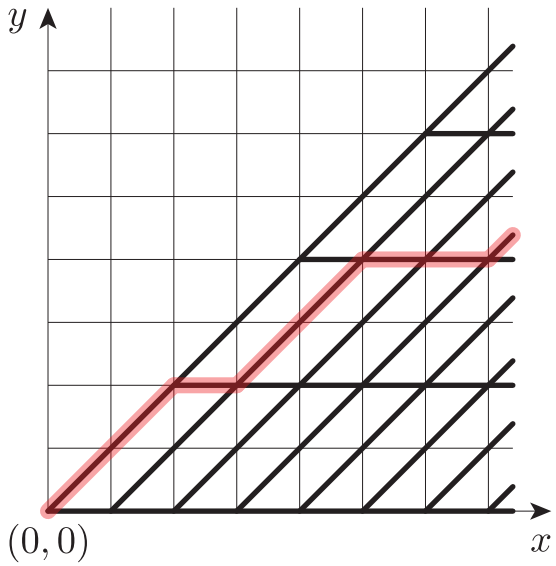

Figure B.1: The lattice and an example of lattice paths on it regarding computing $(E^N)_{(0,0)(l,l)}$. Each path is from $(0,0)$ to (N,l) with l up-steps $\nearrow$ and $(N-l)$ horizontal steps $\rightarrow$, but any horizontal steps on odd y lines are prohibited.

BIBLIOGRAPHY

[1] A. Polkovnikov, K. Sengupta, A. Silva, and M. Vengalattore, Rev. Mod. Phys. **83**, 863 (2011).

[2] L. D'Alessio, Y. Kafri, A. Polkovnikov, and M. Rigol, Adv. Phys. **65**, 239 (2016).

[3] S. Trotzky, Y.-A. Chen, A. Flesch, I. P. McCulloch, U. Schollwöck, J. Eisert, and I. Bloch, Nat. Phys. **8**, 325 (2012).

[4] C. Neill *et al.*, Nat. Phys. **12**, 1037 (2016).

[5] T. Kinoshita, T. Wenger, and D. S. Weiss, Nature (London) **440**, 900 (2006).

[6] Y. Tang, W. Kao, K.-Y. Li, S. Seo, K. Mallayya, M. Rigol, S. Gopalakrishnan, and B. L. Lev, Phys. Rev. X **8**, 021030 (2018).

[7] W. Kao, K.-Y. Li, K.-Y. Lin, S. Gopalakrishnan, and B. L. Lev, Science **371**, 296 (2021).

[8] J. Smith, A. Lee, P. Richerme, B. Neyenhuis, P. W. Hess, P. Hauke, M. Heyl, D. A. Huse, and C. Monroe, Nat. Phys. **12**, 907 (2016).

[9] H. Bernien, S. Schwartz, A. Keesling, H. Levine, A. Omran, H. Pichler, S. Choi, A. S. Zibrov, M. Endres, M. Greiner, V. Vuletić, and M. D. Lukin, Nature (London) **551**, 579 (2017).

[10] M. Rigol, V. Dunjko, and M. Olshanii, Nature (London) **452**, 854 (2008).

[11] H. Kim, T. N. Ikeda, and D. A. Huse, Phys. Rev. E **90**, 052105 (2014).

[12] J. R. Garrison and T. Grover, Phys. Rev. X **8**, 021026 (2018).

[13] C. Gogolin and J. Eisert, Rep. Prog. Phys. **79**, 056001 (2016).

[14] T. Mori, T. N. Ikeda, E. Kaminishi, and M. Ueda, J. Phys. B **51**, 112001 (2018).

[15] G. Biroli, C. Kollath, and A. M. Läuchli, Phys. Rev. Lett. **105**, 250401 (2010).

[16] E. Iyoda, K. Kaneko, and T. Sagawa, Phys. Rev. Lett. **119**, 100601 (2017).

[17] L. Boltzmann, Sitzungsberichte Akademie der Wissenschaften **66**, 275 (1872).

[18] J. von Neumann, Z. Phys. **57**, 30 (1929), [Eur. Phys. J. H 35, 201 (2010). (translated by R. Tumulka)].

[19] H. Tasaki, Phys. Rev. Lett. **80**, 1373 (1998).

[20] S. Goldstein, J. L. Lebowitz, R. Tumulka, and N. Zanghì, Phys. Rev. Lett. **96**, 050403 (2006).

[21] S. Popescu, A. J. Short, and A. Winter, Nat. Phys. **2**, 754 (2006).

[22] P. Reimann, Phys. Rev. Lett. **99**, 160404 (2007).

[23] H. Tasaki, J. Stat. Phys. **163**, 937 (2016).

[24] P. Reimann, Nat. Commun. **7**, 10821 (2016).

[25] K. Kaneko, E. Iyoda, and T. Sagawa, Bulletin of Physical Society of Japan **73**, 361 (2018).

[26] M. Rigol, Phys. Rev. Lett. **103**, 100403 (2009).

[27] P. Reimann, Phys. Rev. Lett. **101**, 190403 (2008).

[28] M. Ueda, Nat. Rev. Phys. **2**, 669 (2020).

[29] J. M. Deutsch, Phys. Rev. A **43**, 2046 (1991).

[30] M. Srednicki, Phys. Rev. E **50**, 888 (1994).

[31] T. Mori, (2016), arXiv:1609.09776 .

[32] N. Shiraishi and T. Mori, Phys. Rev. Lett. **119**, 030601 (2017).

[33] J.-S. Caux and J. Mossel, J. Stat. Mech. (2011) P02023.

[34] M. Rigol, V. Dunjko, V. Yurovsky, and M. Olshanii, Phys. Rev. Lett. **98**, 050405 (2007).

[35] W. Beugeling, R. Moessner, and M. Haque, Phys. Rev. E **89**, 042112 (2014).

[36] V. Alba, Phys. Rev. B **91**, 155123 (2015).

[37] T. Yoshizawa, E. Iyoda, and T. Sagawa, Phys. Rev. Lett. **120**, 200604 (2018).

[38] V. E. Korepin, N. M. Bogoliubov, and A. G. Izergin, *Quantum Inverse Scattering Method and Correlation Functions* (Cambridge University Press, 1993).

[39] M. Takahashi, *Thermodynamics of One-Dimensional Solvable Models* (Cambridge University Press, 1999).

[40] L. Tonks, Phys. Rev. **50**, 955 (1936).

[41] M. Girardeau, J. Math. Phys. **1**, 516 (1960).

[42] E. H. Lieb and W. Liniger, Phys. Rev. **130**, 1605 (1963).

[43] E. H. Lieb, Phys. Rev. **130**, 1616 (1963).

[44] P. W. Anderson, Phys. Rev. **109**, 1492 (1958).

[45] A. Pal and D. A. Huse, Phys. Rev. B **82**, 174411 (2010).

[46] R. Nandkishore and D. A. Huse, Annu. Rev. Condens. Matter Phys. **6**, 15 (2015).

[47] D. A. Abanin and Z. Papić, Ann. Phys. **529**, 1700169 (2017).

[48] F. Alet and N. Laflorencie, C.R. Phys. **19**, 498 (2018).

[49] B. Bauer and C. Nayak, J. Stat. Mech. (2013) P09005.

[50] M. Žnidarič, T. Prosen, and P. Prelovšek, Phys. Rev. B **77**, 064426 (2008).

[51] D. J. Luitz, N. Laflorencie, and F. Alet, Phys. Rev. B **91**, 081103(R) (2015).

[52] G. Casati, B. V. Chirikov, and I. Guarneri, Phys. Rev. Lett. **54**, 1350 (1985).

[53] T. Guhr, A. Müller–Groeling, and H. A. Weidenmüller, Phys. Rep. **299**, 189 (1998).

[54] T. Prosen and M. Robnik, J. Phys. A **26**, 2371 (1993).

[55] D. A. Rabson, B. N. Narozhny, and A. J. Millis, Phys. Rev. B **69**, 054403 (2004).

[56] V. Oganesyan and D. A. Huse, Phys. Rev. B **75**, 155111 (2007).

[57] Y. Y. Atas, E. Bogomolny, O. Giraud, and G. Roux, Phys. Rev. Lett. **110**, 084101 (2013).

[58] M. Serbyn, Z. Papić, and D. A. Abanin, Phys. Rev. Lett. **111**, 127201 (2013).

[59] D. A. Huse, R. Nandkishore, and V. Oganesyan, Phys. Rev. B **90**, 174202 (2014).

[60] J. Z. Imbrie, J. Stat. Phys. **163**, 998 (2016).

[61] J. Z. Imbrie, Phys. Rev. Lett. **117**, 027201 (2016).

[62] M. Schreiber, S. S. Hodgman, P. Bordia, H. P. Lüschen, M. H. Fischer, R. Vosk, E. Altman, U. Schneider, and I. Bloch, Science **349**, 842 (2015).

[63] S. Zhang, M. Karbach, G. Müller, and J. Stolze, Phys. Rev. B **55**, 6491 (1997).

[64] C. D. Batista and G. Ortiz, Phys. Rev. Lett. **85**, 4755 (2000).

[65] T. Rakovszky, P. Sala, R. Verresen, M. Knap, and F. Pollmann, Phys. Rev. B **101**, 125126 (2020).

[66] W. Caspers and P. Iske, Physica A **157**, 1033 (1989).

[67] P. Sala, T. Rakovszky, R. Verresen, M. Knap, and F. Pollmann, Phys. Rev. X **10**, 011047 (2020).

[68] S. Scherg, T. Kohlert, P. Sala, F. Pollmann, H. M. Bharath, I. Bloch, and M. Aidelsburger, Nat. Commun. **12**, 4490 (2021).

[69] M. Serbyn, D. A. Abanin, and Z. Papić, Nat. Phys. **17**, 675 (2021).

[70] S. Moudgalya, B. A. Bernevig, and N. Regnault, (2021), arXiv:2109.00548 .

[71] N. Robinson, Physics **11**, 105 (2018).

[72] E. J. Heller, Phys. Rev. Lett. **53**, 1515 (1984).

[73] L. A. Bunimovich, Comm. Math. Phys. **65**, 295 (1979).

[74] M. Srednicki, Phys. Rev. Lett. **71**, 666 (1993).

[75] P. Calabrese and J. Cardy, J. Stat. Mech. (2004) P06002.

[76] M. B. Hastings, J. Stat. Mech. (2007) P08024.

[77] R. Orús, Ann. Phys. (Amsterdam) **349**, 117 (2014).

[78] C. J. Turner, A. A. Michailidis, D. A. Abanin, M. Serbyn, and Z. Papić, Nat. Phys. **14**, 745 (2018).

[79] C. J. Turner, A. A. Michailidis, D. A. Abanin, M. Serbyn, and Z. Papić, Phys. Rev. B **98**, 155134 (2018).

[80] D. Jaksch, J. I. Cirac, P. Zoller, S. L. Rolston, R. Côté, and M. D. Lukin, Phys. Rev. Lett. **85**, 2208 (2000).

[81] C.-J. Lin and O. I. Motrunich, Phys. Rev. Lett. **122**, 173401 (2019).

[82] T. Mori and N. Shiraishi, Phys. Rev. E **96**, 022153 (2017).

[83] C. K. Majumdar and D. K. Ghosh, J. Math. Phys. **10**, 1388 (1969).

[84] C. K. Majumdar and D. K. Ghosh, J. Math. Phys. **10**, 1399 (1969).

[85] M. Schecter and T. Iadecola, Phys. Rev. Lett. **123**, 147201 (2019).

[86] S. Chattopadhyay, H. Pichler, M. D. Lukin, and W. W. Ho, Phys. Rev. B **101**, 174308 (2020).

[87] T. Iadecola and M. Schecter, Phys. Rev. B **101**, 024306 (2020).

[88] D. K. Mark and O. I. Motrunich, Phys. Rev. B **102**, 075132 (2020).

[89] S. Moudgalya, N. Regnault, and B. A. Bernevig, Phys. Rev. B **102**, 085140 (2020).

[90] N. O'Dea, F. Burnell, A. Chandran, and V. Khemani, Phys. Rev. Research **2**, 043305 (2020).

[91] K. Bull, J.-Y. Desaules, and Z. Papić, Phys. Rev. B **101**, 165139 (2020).

[92] I. Affleck, T. Kennedy, E. H. Lieb, and H. Tasaki, Phys. Rev. Lett. **59**, 799 (1987).

[93] I. Affleck, T. Kennedy, E. H. Lieb, and H. Tasaki, Comm. Math. Phys. **115**, 477 (1988).

[94] H. Tasaki, *Physics and Mathematics of Quantum Many-Body Systems* (Springer, Berlin, 2020).

[95] F. Pollmann, A. M. Turner, E. Berg, and M. Oshikawa, Phys. Rev. B **81**, 064439 (2010).

[96] F. Pollmann, E. Berg, A. M. Turner, and M. Oshikawa, Phys. Rev. B **85**, 075125 (2012).

[97] X. Chen, Z.-C. Gu, Z.-X. Liu, and X.-G. Wen, Phys. Rev. B **87**, 155114 (2013).

[98] B. Zeng, X. Chen, D.-L. Zhou, and X.-G. Wen, *Quantum information meets quantum matter: From quantum entanglement to topological phases of many-body systems* (Springer, New York, 2019).

[99] S. Moudgalya, S. Rachel, B. A. Bernevig, and N. Regnault, Phys. Rev. B **98**, 235155 (2018).

[100] S. Moudgalya, N. Regnault, and B. A. Bernevig, Phys. Rev. B **98**, 235156 (2018).

[101] D. K. Mark, C.-J. Lin, and O. I. Motrunich, Phys. Rev. B **101**, 195131 (2020).

[102] F. D. M. Haldane, Phys. Lett. **93 A**, 464 (1983).

[103] F. D. M. Haldane, Phys. Rev. Lett. **50**, 1153 (1983).

[104] H. Katsura, private communication.

[105] A. O. Barut and A. Böhm, Phys. Rev. **139**, B1107 (1965).

[106] C. N. Yang, Phys. Rev. Lett. **63**, 2144 (1989).

[107] S. Zhang, Phys. Rev. Lett. **65**, 120 (1990).

[108] C. N. Yang and S. Zhang, Mod. Phys. Lett. B **4**, 759 (1990).

[109] L. Onsager, Phys. Rev. **65**, 117 (1944).

[110] E. Lieb, T. Schultz, and D. Mattis, Ann. Phys. **16**, 407 (1961).

[111] S. Katsura, Phys. Rev. **127**, 1508 (1962).

[112] L. V. Avdeev and A. A. Vladimirov, Theor. Math. Phys. **69**, 1071 (1986).

[113] F. H. L. Essler, V. E. Korepin, and K. Schoutens, J. Phys. A **25**, 4115 (1992).

[114] J. D. Noh, D.-S. Lee, and D. Kim, Physica A **287**, 167 (2000).

[115] R. I. Nepomechie and C. Wang, J. Phys. A **46**, 325002 (2013).

[116] V. Alba, M. Fagotti, and P. Calabrese, J. Stat. Mech. (2009) P10020.

[117] H. W. Gould, Amer. Math. Monthly **63**, 84 (1956).

[118] D. Applebaum, *Probability and Information: An Integrated Approach* (Cambridge University Press, Cambridge, UK, 2008).

[119] D. N. Page, Phys. Rev. Lett. **71**, 1291 (1993).

[120] I. Lesanovsky, Phys. Rev. Lett. **106**, 025301 (2011).

[121] E. Vernier, E. O'Brien, and P. Fendley, J. Stat. Mech. (2019) 043107.

[122] M. Suzuki, Prog. Theor. Phys. **56**, 1454 (1976).

[123] L. Dolan and M. Grady, Phys. Rev. D **25**, 1587 (1982).

[124] B. Davies, J. Phys. A **23**, 2245 (1990).

[125] B. Davies, J. Math. Phys. **32**, 2945 (1991).

[126] A. B. Zamolodchikov and V. A. Fateev, Sov. J. Nucl. Phys **32**, 298 (1980).

[127] A. G. Bytsko, J. Math. Phys. **44**, 3698 (2003).

[128] K. Mizuta, K. Takasan, and N. Kawakami, Phys. Rev. Research **2**, 033284 (2020).

[129] B. Mukherjee, S. Nandy, A. Sen, D. Sen, and K. Sengupta, Phys. Rev. B **101**, 245107 (2020).

[130] S. Sugiura, T. Kuwahara, and K. Saito, Phys. Rev. Research **3**, L012010 (2021).

[131] D. B. Uglov and I. T. Ivanov, J. Stat. Phys. **82**, 87 (1996).

[132] A. Kuniba and V. Pasquier, Nucl. Phys. B **949**, 114792 (2019).

[133] B. van Voorden, M. Marcuzzi, K. Schoutens, and J. Minář, Phys. Rev. B **103**, L220301 (2021).

[134] R. W. Chhajlany, P. R. Grzybowski, J. Stasińska, M. Lewenstein, and O. Dutta, Phys. Rev. Lett. **116**, 225303 (2016).

[135] A. Hudomal, I. Vasić, N. Regnault, and Z. Papić, Commun. Phys. **3**, 99 (2020).

[136] L. Gotta, L. Mazza, P. Simon, and G. Roux, Phys. Rev. B **104**, 094521 (2021).